Kinetics of Aggregation and Gel Formation in Concentrated Polystyrene Colloids

Peter Sandkühler, Jan Sefcik, and Massimo Morbidelli*

Swiss Federal Institute of Technology Zurich, Institut für Chemie- und Bioingenieurswissenschaften, ETH-Hönggerberg/HCI, CH-8093 Zurich, Switzerland

Received: August 6, 2004; In Final Form: September 29, 2004

We measure with dynamic and static light scattering the radius of gyration, the hydrodynamic radius at various angles, and the average structure factor and determine the kinetic behavior for aggregation processes of a polystyrene colloid at moderately concentrated solid volume fractions $\phi_0 \leq 0.1$ and various salt concentrations. In addition, we measure the gelation kinetics in these colloidal dispersions at volume factions $\phi_0 \geq 0.05$ using on-line oscillatory shear measurements. By modifying the surface of the sodium dodecyl sulfate stabilized polystyrene particles with Triton X-100, we show that the changed interaction potential is responsible for a clear change in the aggregation behavior and kinetics as well as in the gelation kinetics and gel properties. We demonstrate that the measured aggregation kinetics can be accurately described by population balance equations, i.e., the Smoluchowski aggregation equation, at all solid volume fractions investigated. The model for the aggregate structure allows us to distinguish between different fractal dimensions through comparison to the measured average structure factor. It is found that the structure of the aggregates is best described by a small fractal dimension of 1.8 and a power-law growth of the average radii. This is surprising for the relatively slow reaction-limited cluster aggregation regime with stability ratios of $W \sim 1 \times 10^6$. A kinetic scaling in the aggregation behavior, independent of the salt concentration and the volume fraction, is found through a dimensionless time derived from the rate equations. Remarkably, the time evolution of the gel elastic modulus could also be scaled by the dimensionless time derived from the aggregation model. This finding suggests that the kinetics of gel formation still can be described as a second-order rate process, like aggregation, even for very concentrated systems close to the gel point.

1. Introduction and Motivation

Aggregation of colloidal particles, the corresponding kinetics, and the resulting aggregate structures have been the topic of intensive research over the last 15 years leading to an extensive literature (cf. refs 1−23). These works deal mostly with the kinetics of aggregation in very dilute systems. In these conditions, multiple scattering is negligible and light scattering techniques can be used to monitor in situ the time evolution of the system and the obtainable measurables can be quantitatively interpreted. Convenient mathematical tools, like the Smoluchowski aggregation equation, can be used to model the aggregation kinetics at sufficiently low volume fractions. Although denser systems are of great practical and industrial interest,[24−29] only a limited number of investigations on the aggregation kinetics at higher solid volume fractions have been reported.[30,31] The so far limited progress in the kinetic modeling of aggregation and gelation can be attributed to the fact that in these conditions both the experimental and the modeling analysis become more demanding.[32−36] In addition, gel formation often occurs in more concentrated systems,[37−50] which adds further complexity to the aggregation process itself. In recent work,[51] experiments employing fiber-optics based dynamic light scattering in the backscattering geometry together with linear-viscoelastic oscillatory rheology on slowly aggregating and gelling acrylic latexes at concentrated solid volume fractions of 17% and 23% have been reported. Through measurements of various power-law exponents, the analogy of colloidal gelation to polymer gelation has been tested and some consistent features have been found.

However, there is a lack of quantitative studies in order to understand when (in time) this liquid−solid transition in colloidal systems occurs and how the aggregation kinetics preceding the gel formation can be described. Several studies investigated gel transitions on a purely mathematical basis, the so-called mathematical gelation, in the frame of the Smoluchowski aggregation equation (cf. refs 52 and 53). However, the aggregation models typically required to produce such mathematical gels are in general not applicable to colloidal dispersions undergoing aggregation and gelation, as can be seen by comparison with appropriate experimental data.[54]

It is thus evident that quantitative and predictive kinetic models of aggregation and gelation would be very useful for many practical and industrial applications to produce aggregates and gels of desired size and structure.[35,55−58] In our recent work, we have investigated the problem of modeling the kinetics of aggregation in nondilute dispersions, where aggregation might result in gel formation.[54,59−61] In this work, we report and analyze new aggregation and gelation experiments in order to rationalize and quantify the kinetics of slow aggregation and gelation at higher solid volume fractions up to $\phi_0 \leq 0.1$, using a typical polystyrene colloid. In previous work,[54] we have investigated the same colloid in more diluted conditions in the DLCA regime, where a behavior typical for DLCA was observed. Here, light scattering and oscillatory shear measurements are used to characterize the aggregation progress. In particular, several averages of the aggregate mass distribution

* To whom correspondence should be addressed.

10.1021/jp046468w CCC: $27.50
Published on Web 11/26/2004

TABLE 1: Expressions for the Structure Factor, $S_i(Q)$, the Radius of Gyration, $R_{g,i}/R_p$, and the Hydrodynamic Radius, $R_{h,i}/R_p$, of Primary Particles, Dimers, Trimers, and Tetramers[a]

Cluster	$S_i(Q)$	$R_{g,i}/R_p$	$R_{h,i}/R_p$
Monomer	1	$\sqrt{\frac{3}{5}}$	1
Dimer	$0.5(1+\frac{\sin(2Q)}{2Q})$	$\sqrt{\frac{8}{5}}$	1.38
Trimer	$\frac{1}{9}(3+4\frac{\sin(2Q)}{2Q}+\frac{\sin(2Q\delta)}{2Q\delta})$ $\delta=2\sqrt{2-2\cos(103^o)}$	$\sqrt{\frac{107-40\cos(103^o)}{45}}$	1.89
Tetramer	$\frac{1}{16}(4+6\frac{\sin(2Q)}{2Q}+2\frac{\sin(s_{23}Q)}{s_{23}Q}+$ $...2\frac{\sin(s_{24}Q)}{s_{24}Q}+2\frac{\sin(s_{34}Q)}{s_{34}Q})$	$\sqrt{(\frac{3}{5}+\frac{12+s_{23}^2+s_{24}^2+s_{34}^2}{16})}$	$\frac{4}{1+0.5(\frac{3}{2}+\frac{1}{s_{23}}+\frac{1}{s_{24}}+\frac{1}{s_{34}})}$

[a] The values of $s_{ij} = r_{ij}/(2R_p)$ are given in Table 2.

TABLE 2: Values of the Average Normalized Interparticle Distances $s_{ij} = r_{ij}/(2R_p)$ for Tetramers, in the Case of $d_f = 2.05$ and $d_f = 1.85$[63]

	$d_f = 1.85$	$d_f = 2.05$
s_{12}	1	1
s_{13}	1	1
s_{14}	1	1
s_{23}	1.3942	1.3756
s_{24}	1.6798	1.6625
s_{34}	2.0614	2.0347

have been measured as a function of time in order to gain more detailed information on its shape and width. The analysis of the aggregation process is conducted using detailed population balance equation and light scattering models.

2. Theoretical Background

2.1. Dimensionless Structure and Properties of Single Aggregates. The fractal scaling concept can often be used to characterize the structure of clusters created through aggregation in quiescent suspensions. Therein, the dimensionless radius of gyration, $\rho_{g,i}$, of a fractal cluster is related to its dimensionless mass i through the fractal dimension d_f

$$i = k_f\left(\frac{R_{g,i}}{R_p}\right)^{d_f} \equiv k_f(\rho_{g,i})^{d_f} \tag{1}$$

where R_p is the primary particle radius, $R_{g,i}$ the radius of gyration of an aggregate of mass i, and k_f the fractal prefactor. However, the aggregates produced in concentrated systems are relatively small and contain less than 100 primary particles. In this case, the applicability of eq 1 and of the general concept of fractal geometry can be questioned. For example, it has been shown in the context of colloidal gels[62] obtained at $\phi_0 > 0.01$ that the nonfractal part, due to the smaller aggregates, influences significantly the apparent fractal dimension estimated from the average structure factor $\langle S(q)\rangle$ measured by static light scattering. Since in this work we use light scattering measurements to characterize the mass distribution of the aggregate as well as their structure, we need to properly account for the deviations from the fractal behavior exhibited by the smaller clusters.

Explicit dimensionless expressions for the individual cluster structure factor, the radius of gyration ($\rho_{g,i} = R_{g,i}/R_p$) and the hydrodynamic radius ($\rho_{h,i} = R_{h,i}/R_p$) for aggregates composed of less than five particles, are summarized in Tables 1 and 2.[59]

To describe the structure of aggregates containing five or more primary particles in more detail, the particle−particle correlation function $g(r)$ can be used. A semiempirical model for $g(r)$ has recently been developed using Monte Carlo simulations for DLCA and RLCA aggregates of various aggregate sizes.[63−66] Its dimensionless form is given by

TABLE 3: Values of the Parameters d, e, f, and m to Be Used in Equation 3, to Compute the Parameters of the Particle−Particle Correlation Function: N_i^{nn}, a_i, b_i, and γ_i, as a Function of the Number of Particles Per Cluster for Both $d_f = 1.85$ and $d_f = 2.05$[63]

F_i	aggregation mechanism	d	e	f	m
N_i^{nn}	$d_f = 1.85$	2.0342	1.1477	0.9997	1
	$d_f = 2.05$	2.0415	1.1511	1.0086	1
a_i	$d_f = 1.85$	0.0095	4.1292	0.1997	2
	$d_f = 2.05$	0.0138	2.7544	4.1792	2
b_i[a]	$d_f = 1.85$	0.6425	6.2352	5.1747	1
	$d_f = 2.05$	0.4857	9.6836	11.6665	1
γ_i	$d_f = 1.85$	2.1976	3.8377	−0.1784	1
	$d_f = 2.05$	2.16	0.1966	−3.5926	2

[a] $b_i = 0$ for clusters with $d_f = 1.85$ and $i < 7$ or with $d_f = 2.05$ and $i < 10$.

$$\mathcal{F}_{g,i}(s,d_f) \equiv (R_p{}^3 g(r)) = \begin{cases} 0 & \text{if } s < 2 \\ \dfrac{N_i^{nn}}{16\pi}(R_p)^2\delta(s-2) & \text{if } s = 2 \\ a_i s^{b_i} & \text{if } 2 < s < 4 \\ c_i s^{d_f-3}\exp\left(-\left(\dfrac{s}{\xi_i^*}\right)^{\gamma,i}\right) & \text{if } s > 4 \end{cases} \tag{2}$$

where $s = r/R_p$ is the dimensionless distance, while N_i^{nn}, a_i, b_i, and γ_i are empirical dimensionless functions of the cluster mass i and are calculated through the following relation

$$F_i = d\frac{(i-e)^m}{(i-e)^m + f} \tag{3}$$

where the values of the parameters d, e, m, and f[63] are reported in Table 3 for fractal dimensions of $d_f = 1.85$ and 2.05, respectively. The dimensionless constant c_i in eq 2 is given by

$$c_i = \frac{i - 1 - N_i^{nn} - \dfrac{4\pi a_i}{b_i+3}\cdot(4^{b_i+3} - 2^{b_i+3})}{\dfrac{4\pi}{\gamma_i}(\xi_i^*)^{d_f}\Gamma\left(\dfrac{d_f}{\gamma_i}\right)\left(1 - \Gamma_{inc}\left(\left(\dfrac{4}{\xi_i^*}\right)^{\gamma_i}, \dfrac{d_f}{\gamma_i}\right)\right)} \tag{4}$$

The dimensionless cutoff length ξ_i^* in eqs 2 and 4 characterizing the finite size of the cluster can be calculated by

$$\xi_i^* \equiv \frac{\xi_i}{R_p} = \left(\frac{l}{k_f^{1/d_f}}\right) i^{1/d_f} \tag{5}$$

where the constant l has been consistently obtained within this approach to be equal to 0.957 and 0.91 for fractal dimensions of 1.85 and 2.05, respectively.

The structure factor of an aggregate of dimensionless mass i is given by the Fourier transform of $\mathcal{F}_{g,i}(s, d_f)$ in dimensionless form as

$$S_i(Q, d_f) = \frac{1}{i}\left(1 + 4\pi \int_0^\infty s^2 \mathcal{F}_{g,i}(s, d_f)\frac{\sin(Qs)}{Qs}\,ds\right) \quad (6)$$

where Q is the dimensionless scattering wave vector

$$Q \equiv R_p q = R_p \frac{4\pi n}{\lambda_0}\sin(\theta/2) \quad (7)$$

and n is the refractive index of the solvent, λ_0 the wavelength of the incident light, and θ the scattering angle. Two further properties of the aggregates are relevant to compute characteristics of the aggregate distribution that can be estimated from the light scattering measurements. The first one is the radius of gyration which is computed in dimensionless form using $\mathcal{F}_{g,i}(s, d_f)$ as follows

$$\rho_{g,i}{}^2(d_f) \equiv \frac{R_{g,i}{}^2}{R_{g,p}{}^2} = 1 + \frac{1}{2i}(1 + 4\pi \int_0^\infty s^4 \mathcal{F}_{g,i}(s, d_f)\,ds) \quad (8)$$

where $R_{g,p}$ is the primary particle radius of gyration.[63] The second property is the hydrodynamic radius, which can be computed using a simplified theory for the hydrodynamic drag.[64,67] The model provides an explicit equation for the hydrodynamic radius of an aggregate with a structure described by $\mathcal{F}_{g,i}(s, d_f)$, given by

$$\rho_{h,i}(d_f) \equiv \frac{R_{h,i}}{R_p} = i(1 + 4\pi \int_0^\infty s\mathcal{F}_{g,i}(s, d_f)\,ds)^{-1} \quad (9)$$

where R_p is the hydrodynamic radius of primary particles. The analytical equations, which can be obtained for both $\rho_{g,i}(d_f)$ and $\rho_{h,i}(d_f)$ when substituting eq 2 into eqs 8 and 9, respectively, are reported elsewhere.[63,64] Last, the dimensionless radius of the smallest sphere enclosing the aggregate can also obtained from Monte Carlo simulation data[63] and is given by

$$\rho_{c,i}(d_f) = 1.65\sqrt{\frac{3}{5}}\rho_{g,i}(d_f) \quad (10)$$

which is valid for aggregates of more than four particles.

2.2. Dimensionless Aggregation Kinetics. The time evolution of the cluster mass distribution (CMD) can be described by a set of second-order rate equations, the so-called population balance equations (PBE), which account for the formation and loss of aggregates of mass k due to aggregation events and are given by[54,59,63,68]

$$\frac{dN_k}{dt} = \frac{1}{2}\sum_{i+j=k} K_{ij}N_i(t)N_j(t) - \sum_i K_{ik}N_k(t)N_i(t) \quad (11)$$

K_{ij} is the matrix of the aggregation rate constants given by[59,68]

$$K_{ij} = K_B W^{-1} B_{ij} P_{ij}$$

with

$$K_B = 8k_B T/(3\eta)$$

$$W = \frac{K_B}{K_{11}}$$

$$B_{ij} = \frac{1}{4}(R_{h,i}{}^{-1} + R_{h,j}{}^{-1})(R_{c,i} + R_{c,j})$$

$$P_{ij} = (ij)^\lambda \quad (12)$$

where K_B represents the collision rate constant of primary particles due to Brownian motion, k_B being the Boltzmann constant, T the absolute temperature and η the dynamic viscosity of the solvent. The primary particle interactions are summarized in the stability ratio W, which is the ratio between K_B and the actual rate of aggregation between primary particles. In DLCA, W is a function only of the hydrodynamic interactions that occur upon aggregate collision and takes values in the interval [0.5;2].[69] In RLCA, W has to be estimated using suitable techniques from experimental data.[59,70] The matrix B_{ij} denotes the size dependence of the diffusion coefficient and the collision cross section of the aggregates and applies to both DLCA and RLCA, respectively. The experimentally observed increasing reactivity of larger aggregates in RLCA is quantitatively described by the matrix P_{ij},[59,68,71] which is given by the product of the masses of two colliding aggregates to the power of λ. This expression needs to be empirically corrected by restricting its values to the range $P_{ij} \in [1;W]$ so that $K_{ij} \le K_{ij}^{DLCA}$, since the DLCA rate represents the upper limit of the cluster aggregation rate, at least sufficiently far from the gelation point. The exponent λ characterizes how fast the reactivity of aggregates grows with their mass and takes typically values in the interval [0.25;0.5] for RLCA.[2,59,60,68] In contrast, in the case of DLCA we have $\lambda = 0$.[3] Intermediate values of the exponent have been found for other aggregating systems.[16,18,19,59,72−74]

By introducing the following dimensionless time and number density of aggregates of mass k

$$\tau = \frac{K_B N_0 t}{W} \quad (13)$$

and

$$X_k = \frac{N_k}{N_0} \quad (14)$$

where N_0 represents the initial number density of primary particles, the PBE in eq 11 reduces to

$$\frac{dX_k}{d\tau} = \frac{1}{2}\sum_{i+j=k} B_{ij}P_{ij}X_i(\tau)X_j(\tau) - \sum_i B_{ik}P_{ik}X_k(\tau)X_i(\tau) \quad (15)$$

which can easily been seen to be independent of the initial solid volume fraction ϕ_0 and the stability ratio W. In particular, by rewriting the term $B_{ij}P_{ij}$ in dimensionless form we get

$$B_{ij}P_{ij} = \frac{1}{4}(\rho_{h,i}{}^{-1} + \rho_{h,j}{}^{-1})(\rho_{c,i} + \rho_{c,j})(ij)^\lambda \quad (16)$$

where the dimensionless hydrodynamic radius, $\rho_{h,i} = R_{h,i}/R_p$ and the smallest enclosing sphere radius, $\rho_{c,i} = R_{c,i}/R_p$ can be shown using eqs 2 and 8−10 to be functions only of the values of the parameters d_f and λ (and of course of the dimensionless mass). In other words, the solution $X_k(\tau)$ of eq 15 provides the aggregation kinetics for any value of the stability ratio, W and of the initial primary particle solid volume fraction ϕ_0 (or

equivalently their initial number concentration N_0, i.e., $\phi_0 = v_0 N_0 = 4\pi/3\ R_p N_0$), as long as d_f and λ are fixed. We refer to such a solution in the following as the *master aggregation curve* for fixed values of d_f and λ.

2.3. Dimensionless Averages of the CMD. The calculated time dependent CMD, i.e., $X_i(\tau)$, is used to compute several dimensionless ensemble averaged quantities that are experimentally measured using dynamic and static light scattering.[2,3,59,68] First, the dimensionless average structure factor is obtained by intensity weighted averaging of the individual cluster structure factors given by eq 6

$$\langle S(Q,\lambda, d_f)\rangle = \frac{\sum_i i^2 X_i(\lambda, d_f) S_i(Q, d_f)}{\sum_i i^2 X_i(\lambda, d_f)} \tag{17}$$

where we have explicitly indicated the parameters affecting the average structure factor. Similarly, the dimensionless average radius of gyration is given by

$$\langle \rho_g{}^2(\lambda, d_f)\rangle = \frac{\langle R_g{}^2\rangle}{R_{g,p}{}^2} = \frac{\sum_i i^2 X_i(\lambda, d_f)\rho_{g,i}{}^2(d_f)}{\sum_i i^2 X_i(\lambda, d_f)} \tag{18}$$

where $\rho_{g,i}$ is the dimensionless radius of gyration of an aggregate of i primary particles given by eq 8. The dimensionless hydrodynamic radius $\langle \rho_{h,eff}\rangle$ is a more complex average and depends on the shape of the CMD, the scattering wave vector, the rotational diffusion, the structure of the aggregates, and their internal dynamics.[75] These effects can be accounted for by the following equations:[2,3,76,77]

$$\langle \rho_{h,eff}(\lambda, d_f, Q)\rangle = \frac{\langle R_{h,eff}\rangle}{R_p} = \frac{\sum_i i^2 X_i(\lambda, d_f) S_i(Q, d_f)}{\sum_i i^2 X_i(\lambda, d_f) S_i(Q, d_f)\Omega_{h,eff,i}{}^{-1}(Q, d_f)} \tag{19}$$

$$\Omega_{h,eff,i}{}^{-1}(Q, d_f) = \frac{R_{h,i}}{R_{h,i,eff}} = 1 + \frac{1}{2(\beta_i(d_f))^2}\left(1 + \frac{3\partial \ln S_i(Q, d_f)}{\partial\left(\sqrt{\frac{3}{5}}Q\rho_{g,i}(d_f)\right)^2}\right) + \frac{d_f\rho_{h,i}}{3\rho_{g,i}}(Q\rho_{g,i} - 1) \tag{20}$$

In the second equation the derivative of the logarithm of the structure factor needs to be calculated and is given by

$$\frac{\partial \ln S_i(Q, d_f)}{\partial\left(\sqrt{\frac{3}{5}}Q\rho_{g,i}(d_f)\right)^2} = \frac{4\pi}{\frac{6}{5}Q^2 i\rho_{g,i}(d_f) S_i(Q, d_f)} \times \int_0^\infty s^2 \mathcal{T}_{g,i}(s, d_f)\left(\frac{\sqrt{\frac{3}{5}}Qs\cos\left(\sqrt{\frac{3}{5}}Qs\right) - \sin\left(\sqrt{\frac{3}{5}}Qs\right)}{\sqrt{\frac{3}{5}}Qs}\right) ds \tag{21}$$

where the integral is performed numerically for the different parts in eq 2. The factor $(\beta_i)^2$ in eq 20 also deserves some comments. This in fact includes the effect of the dimensionless translational and rotational hydrodynamic radii and the dimensionless radius of gyration as follows:[65,78]

TABLE 4: Values of the Parameters *d*, *e*, *f*, and *m* to Be Used in Equation 3, to Compute the Ratio between the Rotational Hydrodynamic Radius and the Translational Hydrodynamic Radius, $R_{h,r,i}/R_{h,i}$, as a Function of the Number of Particles Per Cluster for Both DLCA and RLCA[65]

F_i	aggregation mechanism	*d*	*e*	*f*	*m*
$R_{h,r,i}/R_{h,i}$	$d_f = 1.85$	1.2355	0.4558	0.8815	1
	$d_f = 2.05$	1.227	0.2324	0.9172	1

$$(\beta_i(d_f))^2 = \frac{\rho_{h,r,i}{}^3(d_f)}{\rho_{g,i}(d_f)\rho_{h,i}{}^2(d_f)} \tag{22}$$

The dimensionless rotational hydrodynamic radius $\rho_{h,r,i}(d_f) = R_{h,r,i}/R_p$ has been explicitly calculated from clusters generated by Monte Carlo simulations using the Kirkwood-Riseman theory for the cluster friction coefficient.[65] In particular, we used the expression for $F_i = \rho_{h,r,i}/\rho_{h,i}$ in eq 3 with the parameters in Table 4. $\rho_{g,i}$ and $\rho_{h,i}$ are computed as discussed in the context of eqs 8 and 9.

It is worth noting that these different radii, including the dimensionless hydrodynamic radius measured at different angles, can be regarded as different moments of the CMD and therefore provide information on its polydispersity. In addition, by substituting the aggregation master distribution $X_k(\tau)$ into eqs 17−19, it is readily seen that also the kinetics of these quantities is described by master curves, i.e., independent of W and ϕ_0 or N_0. That is for a given aggregation mechanism with fixed λ and d_f, the average radius of gyration and the hydrodynamic radius for a given $Q = qR_p$ are functions only of the dimensionless time τ.

In addition to the above averages, three different types of effective volume fractions occupied by the aggregating clusters can be computed from the CMD. These quantities are defined as the sum of the volumes occupied by each individual aggregate multiplied by the number of such aggregates per unit volume

$$\phi_x(\lambda, d_f, \phi_0) = \phi_0 \sum_i X_i(\lambda, d_f)\rho_{x,i}{}^3(d_f) \tag{23}$$

where, depending on the occupied volume of interest, either the dimensionless radius of the enclosing sphere $\rho_{c,i}(d_f)$ (10), the dimensionless radius of gyration $\rho_{g,i}(d_f)$ (8), or the dimensionless hydrodynamic radius $\rho_{h,i}(d_f)$ (9) can be used to compute ϕ_x. The volume fraction ϕ_c is useful in quantifying when the increasing crowding brings clusters in close vicinity to each other so that overlap and interpenetration among them starts. On the other hand, ϕ_g characterizes a space filling where the inner parts of the aggregates, where most of the cluster mass is located, come into closer vicinity and thus accounts for the crowding of the system in terms of the radii of inertia of the fractal aggregates. Finally, ϕ_h can be helpful in evaluating whether the increasing crowding in the system has an influence on the diffusive properties of the clusters. At time $t = 0$, since only primary particles are present, the hydrodynamic and enclosing sphere radius coincide with the radius of the primary particles so that $\phi_c = \phi_h = \phi_0 = 4\pi R_p{}^3 N_0/3$, whereas the volume fraction for the radius of gyration is slightly smaller, i.e., $\phi_g = (3/5)^{3/2}\phi_0$.

It is worth noting from eq 23 that these average volume fractions are not scaled quantities of the aggregating system and explicitly depend on ϕ_0, although not on W. The relevance

of the absolute magnitude of ϕ_0 for the aggregation process is illustrated by the fact that at $\phi_0 \rightarrow 0$ aggregated colloidal systems are fluidlike, whereas at $\phi_0 \geq 0.01$, they typically undergo gelation.

3. Experimental Section

3.1. Light Scattering. The light scattering measurements (both static and dynamic) were performed using a BI-200SM instrument (Brookhaven) with an argon laser (Lexel 95−2) (wavelength $\lambda_0 = 514.4$ nm), with an angular range of the goniometer from 8° to 150° and a BI-9000 AT digital autocorrelator. The incident light is vertically polarized and a vertical polarizer is mounted in front of the detector.

3.1.1. Static Light Scattering. In a static light scattering experiment, we measure the average intensity, I, at a given scattering angle θ. The angle is related to the scattering wave vector by eq 7. The angular distribution of the scattered light contains information about the structure of the colloidal system, in this case primary particles and clusters. The structural information concerning the shape of the primary particles is described by the form factor, $P(q)$, within the RDG-Theory, which for primary particles fulfilling the conditions $(4\pi R_p/\lambda_0)|m_r - 1| \ll 1$ and $|m_r - 1| \ll 1$, where m_r is the ratio of the refractive index inside to that outside the particle, can be described[79,80] by

$$P(q) = \left(3\frac{\sin(qR_p) - qR_p\cos(qR_p)}{(qR_p)^3}\right)^2 \quad (24)$$

The structural information concerning the clusters is typically described by the average structure factor, $\langle S(q)\rangle$, which for fractal aggregates often shows a power-law dependence on the scattering wave vector q,[2,3] assuming that the aggregates are large enough and thus their fractal properties are well developed. The measured scattered intensity as a function of the wave vector is related to the form and average structure factor[79−81] by

$$\frac{I(q)}{I(0)} = \langle S(q)\rangle P(q) \quad (25)$$

In addition to the average structure factor we obtain from the static light scattering data the average radius of gyration $\langle R_g\rangle$ by using the Zimm plot[82]

$$\frac{1}{\langle S(q)\rangle P(q)} = 1 + \frac{1}{3}q^2\langle R_g^2\rangle \quad (26)$$

where the inverse of the measured intensity is plotted versus the square of the scattering wave vector.

3.1.2. Dynamic Light Scattering. In a dynamic light scattering experiment, we measure the fluctuations in time of the scattered light at a certain scattering wave vector q. These random fluctuations in our case originate from the random movement of the particles and clusters in the solution. To analyze these random fluctuations, we perform an autocorrelation analysis of the time dependent scattered intensity. The measured direct autocorrelation function is normalized with the baseline to obtain the normalized intensity weighted time averaged autocorrelation function defined as[79,83]

$$g_T^{(2)}(q, t) = \frac{\langle I(q, 0)I(q, t)\rangle_T}{\langle I(q)\rangle_T^2} \quad (27)$$

where $\langle\rangle_T$ denotes the average over the time interval T. The data for $g_T^{(2)}(q, t)$ are typically analyzed with the cumulant analysis method, where the logarithm of $[g_T^{(2)}(q, t) - 1]^{0.5}$ is plotted versus t. The autocorrelation function is analyzed by fitting the following third-order polynomial to the experimental data[3]

$$\ln[g_T^{(2)}(q, t) - 1]^{0.5} = 1 - \Gamma_1 t + 0.5\Gamma_2 t^2 - (1/6)\Gamma_3 t^3 \quad (28)$$

The so-called first cumulant Γ_1 is defined and calculated from

$$\Gamma_1 = -[\partial\ln[g_T^{(2)}(q, t) - 1]^{0.5}/\partial t]|_{t\rightarrow 0} \quad (29)$$

This is related to the effective diffusion coefficient of the aggregate or particle population and to its effective hydrodynamic radius as follows:

$$\frac{\Gamma_1}{q^2} = \langle D_{eff}\rangle = \frac{k_B T}{6\pi\eta\langle R_{h,\,eff}\rangle} \quad (30)$$

where the Stokes−Einstein relation has been used.

3.2. Colloidal System and Experimental Protocols. *3.2.1. Preparation of the Polystyrene Colloid.* The polystyrene latex was prepared by emulsion polymerization[84] in our laboratory. The procedure has been described in detail elsewhere.[85] A typical batch polymerization recipe is composed of 4 g of sodium dodecyl sulfate ($C_{12}H_{25}SO_4Na$, SDS, Fluka) dissolved in 480 g of distilled water to which 120 g of styrene monomer (Fluka) were added. The resulting emulsion was stirred at 500 rpm, stripped by nitrogen to remove oxygen and further kept under nitrogen atmosphere. The reaction temperature of the batch was set at 70 °C and polymerization was initiated by adding 0.6*g* of sodium peroxydisulfate ($Na_2S_2O_8$, Fluka), dissolved in a small amount of distilled water. The polymerization was monitored through temperature control of the cooling jacket of the reactor (exothermic reaction). The obtained latex was stripped with nitrogen in order to eliminate any residual monomer.

The mean particle hydrodynamic radius was $R_{h,p} = 33$ nm, measured with dynamic light scattering (DLS) at an angle of 90°. The density of the particles is the typical one for polystyrene with $\rho = 1.05$ kg/L, so that in aggregation experiments buoyancy matching is possible through the use of heavy water (D_2O).[43,54,86] A stock dispersion of polystyrene latex with a solid volume fraction $\phi_0 = 0.18$, referred to as PS−SDS in the following, has been used for all the experiments. This value has been calculated from the weight fraction, determined from the dried solid mass (including polymer, initiator and surfactant), through the knowledge of the respective densities. No further cleaning or dialysis of the latex has been performed.

An important aspect with respect to the colloidal stability of this latex is the pH.[70,87] In Figure 1, the pH of the latex is shown as a function of the solid volume fraction, where the same stock latex has been diluted with deionized water (milli-Q (Millipore)). This acidic pH values can be explained by considering that the sulfate groups on the polymer surface can react in the presence of a strong oxidizer, i.e., the initiator sodium peroxydisulfate, with water[87,88] leading to sulfuric acid and to hydroxy and carboxylated groups on the polymer surface

$$\bullet(M)_n - OSO_4^- + H_2O \rightarrow \bullet(M)_n - OH + H_2SO_4$$

$$\bullet(M)_n - OH + 2S_2O_8^{2-} + H_2O \rightarrow \bullet(M)_{(n-0.5)} - COOH + 4HSO_4^- \quad (31)$$

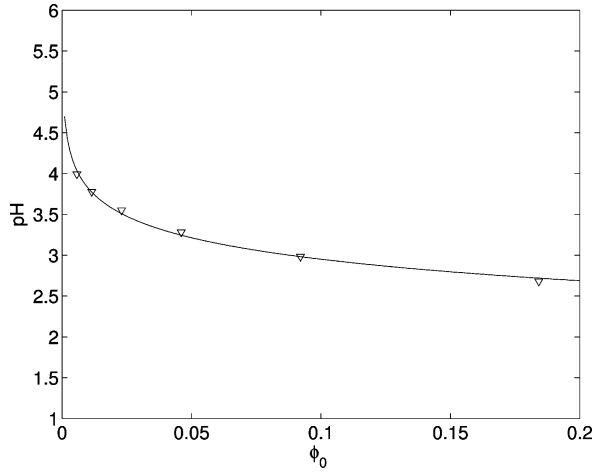

Figure 1. pH measured as a function of the solid volume fraction, ϕ_0 upon dilution of the original stock latex. The line is a fit based on a linear relation between ϕ_0 and the H^+ concentration.

We confirmed in separate experiments that the acidity originates from the peroxydisulfate initiator.

3.2.2. Aggregation Experiments. The aggregation experiments were performed at solid volume fractions of $\phi_0 = 0.09$, 0.05, 0.01, and 0.005. The sodium chloride concentrations used to destabilize the latex in order to initiate aggregation were in the range of 0.24−0.5 mol/L. The latex stock ($\phi_0 = 0.18$) has been, where necessary, diluted to twice the volume fraction desired for the experiments. All dilutions were done with deionized water (milli-Q (Millipore)). A concentration of twice the desired salt solution concentration has been prepared in heavy water, so that the final batch for aggregation was approximately density matched. In any case, for the cluster sizes and volume fractions investigated in this work, the effect of sedimentation can be safely neglected.[59]

The aggregation experiments have been performed as follows. After the necessary pre-dilution steps, equal volumes of colloid and salt solution are mixed to obtain the intended volume fraction ϕ_0. The salt concentrations were selected so as to lead to aggregation rates sufficiently slow to be monitored within 10 h.

At chosen sampling times, samples of 0.1 mL were taken from the aggregating dispersion. The sampling was very carefully done with a pipet in order to minimize shear during withdrawal. The samples were first diluted into 20 mL deionized water and, in a second dilution step, 0.5 mL were again diluted into 10−20 mL deionized water. The exact protocol depended on the initial ϕ_0 and aggregation extent, and the dilution factors were chosen in order to result in transparent dispersions suitable for light scattering measurements.

It is worth noting that the aim of these experiments is to monitor the evolution of the CMD during the aggregation process. The dilution of the sample is needed for two reasons: on one hand, to be able to take suitable light scattering measurements which can be interpreted with the model (17−22), and on the other hand, to stop the aggregation process. Regarding the latter, no change in the measured averages of the CMD has been detected over several weeks at the dilution levels used in this work.

We note that this dilution procedure could in principle change the CMD if the aggregation process is reversible. In this case a decrease of the effective aggregate size upon dilution would be expected. To check this point the dilution procedure has been repeated with different dilution factors in the range from 10 to 1000, and the hydrodynamic radius at an angle of 90° has been measured in each case. No change in the average aggregate size was observed thus indicating the effective irreversibility of the aggregation process under examination. Another disturbance to the CMD can originate from the shear forces acting on the aggregates during sampling with a pipet. We have estimated these shear stresses to be smaller than 1 dyn/cm^2. This value is significantly smaller than values reported in the literature[89] to cause changes in the aggregate structure, though not even breaking them. It is interesting to note that these shear stresses are also significantly smaller than those required to cause strain hardening or rupture of the gels in the rheological measurements reported below. One last point worth pointing out is that experimental difficulties limit the applicability of this procedure to effectively occupied volume fractions ϕ_x not larger than a certain value where early gelation is induced in the sampling pipet.

3.2.3. Polystyrene Colloid Co-stabilized with a Nonionic Surfactant. To investigate the effect of colloidal stability and in particular a different surface chemistry on the aggregation/gelation process we have prepared a second latex, in the following referred to as PS−SDS-Triton, by adding to the original PS−SDS latex a nonionic surfactant. We used Triton X-100 ($M_w = 624$ g/mol, chromatography grade from Merck) as received. The surfactant solution has been pre-diluted in deionized water. Specific amounts of this solution were added to the original latex, resulting in a SDS-Triton X-100 polystyrene latex, whose stability depends on the amount of Triton added. Large amounts stabilize the latex against almost any amount of sodium chloride added to screen the electrical double layer repulsion and to promote aggregation, whereas small amounts have no measurable effect on the stability or aggregation behavior of the latex.[21−23,90] In the aggregation experiments below, we used a colloidal system (PS−SDS-Triton) made by adding an aqueous Triton X-100 solution with a Triton mole fraction of $x_{Triton} = 0.00298$ mol/mol to the PS−SDS colloid to give a mass fraction of $w = 0.0756$ and a colloidal polymer solid volume fraction of $\phi_0 = 0.10$. The so modified latex was kept 12 h to let Triton X-100 adsorb to the polystyrene surface. Thereafter, aggregation was initiated by mixing equal volumes of a salt solution and the modified latex following the protocol of the aggregation experiments described above. Note that also in these aggregation experiments different dilution factors did not result in a decrease of the hydrodynamic radius measured at an angle of 90°. Therefore, at least under these conditions, also the modified polystyrene latex aggregates irreversibly.

3.2.4. Small Amplitude Oscillatory Shearing. To monitor the gel formation and estimate the gelation point, some aggregation experiments have been performed inside a rheometer so as to take in situ linear viscoelastic measurements. A strain controlled rheometer (ARES, Advanced Rheometric Expansion System) from Rheometric Scientific has been used to perform the different measurements on the latexes and gels. This is a couette geometry rheometer with the outer cylinder actuated by a motor and the inner suspended by a torsion wire. The gap between the bob and the outer cylinder is 1 mm (inner radius is 17 mm and outer one 16 mm), and the bob length is 34 mm. The rotating cylinder is temperature controlled at $T = 25 \pm 0.1$ °C in all of the experiments. To prevent evaporation a soaked solvent trap has been attached on the outer rotating cylinder. For very long experiments we have covered this trap with moistened towels to reduce solvent evaporation. The obtained data are analyzed in terms of the elastic ($G'(\omega, t)$) and the loss ($G''(\omega, t)$) modulus as a function of time. Since the measurement time is much shorter than the process characteristic time, these

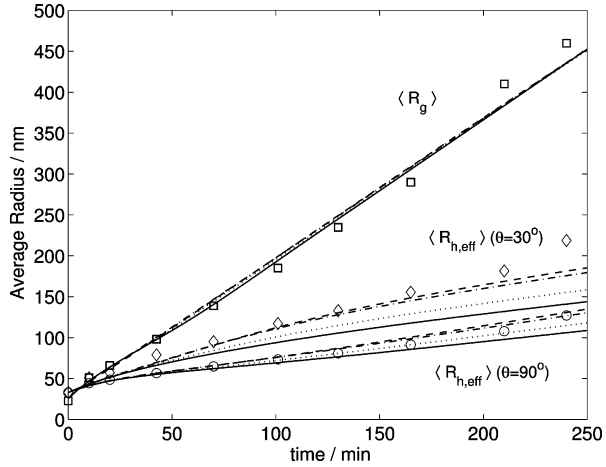

Figure 2. Comparison of the experimental (symbols) average radii as a function of time at $\phi_0 = 0.05$ and [NaCl] = 0.26 mol/L with the model calculations for various fractal dimensions (lines): (- -) $d_f = 2.1$; (− ·) $d_f = 1.95$; (···) $d_f = 1.8$; (−) $d_f = 1.7$.

TABLE 5: RMS Error Calculated with Equation 30 for Several Optimal Triplets of the Parameters d_f, λ, and W, Corresponding to the Data in Figure 2

d_f	λ	W	RMS
2.1	0.225	3.5×10^6	0.0759
1.95	0.200	3.3×10^6	0.0714
1.8	0.163	3.3×10^6	0.0668
1.7	0.140	3.4×10^6	0.0642

measurements can be regarded as instantaneous. The samples were externally mixed to equal amounts of salt solution and latex as in the aggregation experiment and then poured into the couette cup. It is worth noting that extreme care must be taken in lowering the bob in order to minimize shearing. With this precaution the measured time evolution of $G'(\omega, t)$ is well reproducible within 5% variance. Additionally, we measured the frequency and strain dependence of the elastic modulus of the final gels.

4. Results

4.1. Aggregation and Gelation Behavior of PS−SDS Latexes. In this section, we discuss polystyrene latexes stabilized with SDS. We first analyze the aggregation behavior of a particular aggregation experiment, performed at $\phi_0 = 0.05$ and [NaCl] = 0.26 mol/L. In Figure 2, the experimental average radius of gyration and hydrodynamic radii, the latter measured at two angles, $\theta = 30°$ and 90°, are shown as a function of time. Note that in this figure and in the following we show the data of the average radii not made dimensionless with the radius of the primary particles, which in this work is constant anyway, for better readability of the dimensions of the aggregates. The aggregation model contains three a priori unknown parameters: the fractal dimension d_f, the kernel exponent λ, and the stability ratio W. In Figure 2, four model calculations, corresponding to four choices of the fractal dimension, i.e., $d_f = 2.1$ (- -), 1.95 (- ·), 1.8 (···), and 1.7 (−), are compared with the experimental data. In each case, the best pair of values for the parameters λ and W has been determined by fitting the time evolution of the radius of gyration only. The results of this fitting are summarized in Table 5, where for each given value of d_f, the corresponding fitted pair of λ and W values is reported together with the corresponding value of the root-mean-squared error defined by

$$\mathrm{rms} = \sqrt{\frac{1}{(n-1)}\sum_{i=1}^{n}\left(1 - \frac{\langle R_g\rangle_i^{\mathrm{mod}}}{\langle R_g\rangle_i^{\mathrm{exp}}}\right)^2} \qquad i = 1...n \quad (32)$$

where n is the number of experimental points. Note that the calculated rms values indicate that a slightly better fit is obtained for the smallest d_f value when focusing on $\langle R_g\rangle$, although the fitted lines in Figure 2 are hardly distinguishable. However, when comparing also the predictions for the hydrodynamic radii with the experimental data, some differences are observed. In particular, we see that for larger fractal dimensions ($d_f = 2.1$) the fit for both angles is good, for intermediate fractal dimensions ($d_f = 1.95$ and 1.8) the agreement with the data at an angle of 90° becomes better, and at 30°, worse, and finally, for $d_f = 1.7$, the agreement with the experimental data at both angles becomes inferior.

From these results, it can be concluded that for each given value of d_f one combination of λ and W exists that can produce a substantially equivalent fit of the $\langle R_g\rangle$ and to similar extent also of the $\langle R_{h,eff}\rangle$ experimental data. Consequently it is hard to determine unambiguously from these data the correct fractal dimension.

For this we have to consider the comparison between the experimental and calculated average structure factors shown in Figure 3a−d for the four fractal dimensions considered above. It is seen that the agreement between model and experimental data is best for the fractal dimension $d_f = 1.8$. We can therefore conclude that the SDS stabilized polystyrene particles at $\phi_0 = 0.05$ and [NaCl] = 0.26 mol/L aggregate into clusters with a rather small fractal dimension considering that the aggregation proceeds under relatively slow RLCA conditions with a stability ratio of $W = 3.3 \times 10^6$ and a kernel exponent $\lambda = 0.19$.

4.1.1. Role of Solid Volume Fraction and Salt Concentration. The modeling analysis described in the previous section has been repeated for aggregation experiments performed at different salt concentrations, i.e., [NaCl] = 0.24, 0.28, 0.30, and 0.32 mol/L, and at the same solid volume fraction $\phi_0 = 0.05$. In all cases, it was found that the best fit was obtained using $d_f = 1.8$. The results for the average radii are shown in Figure 4a−d and for the corresponding average static structure factors as a function of q in Figure 5a−d. It is seen that a good fitting of the experimental data is obtained in each case.

The measured time evolutions of the average radii measured at a larger solid volume fraction $\phi_0 = 0.09$ for [NaCl] = 0.24 and 0.26 mol/L, are compared in Figure 6, parts a and b, respectively, with the model calculations obtained again by fixing $d_f = 1.8$ and fitting W and λ. The corresponding comparisons for the average structure factor are shown in Figure 6c,d.

Finally, two aggregation experiments have been performed at smaller solid volume fractions, i.e., $\phi_0 = 0.01$ ([NaCl] = 0.32 mol/L) and 0.005 (0.28 mol/L). The obtained experimental results are compared with the model calculations with $d_f = 1.8$ in Figure 7a,b for the average radii and in Figure 7c,d for the average structure factors. The comparison between model calculations and experimental data is in all cases satisfactory.

The values of the parameters λ and W fitted in modeling all the above experimental runs are shown as a function of the salt concentration for different values of the solid volume fraction in Figure 8, parts a and b, respectively. It is seen that the variation of the parameter λ is modest and shows no specific trend with an average value equal to 0.182. The stability ratio instead increases with decreasing solid volume fraction and shows, at least for the data at $\phi_0 = 0.05$, a clear dependence on

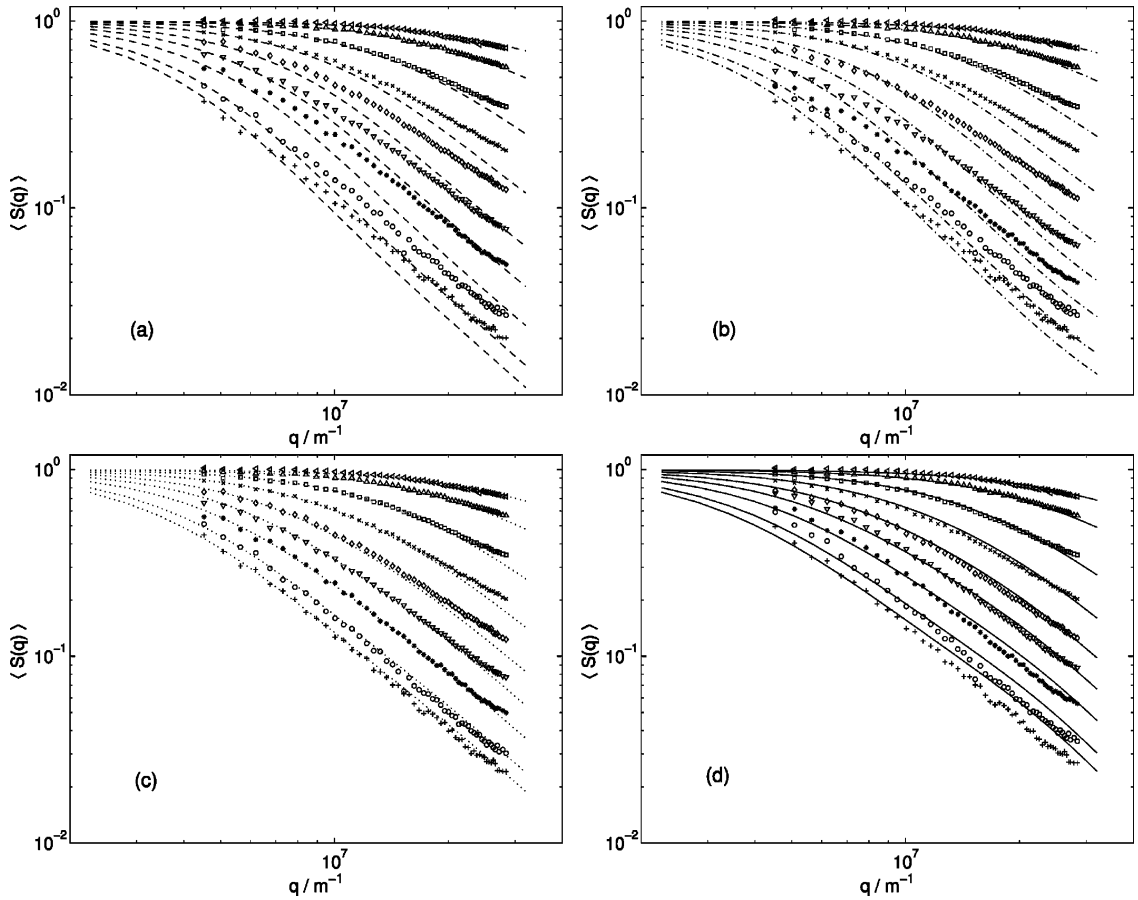

Figure 3. Comparison of the experimental average structure factors (symbols) with the model calculations as a function of q for various aggregation times corresponding to the data in Fig. 2. (a) (− −) $d_f = 2.1$; (b) (− ·) $d_f = 1.95$; (c) (···) $d_f = 1.8$; (d) (−) $d_f = 1.7$. (leftward triangle) $t = 10$, (△) 20, (□) 42, (×) 70, (◇) 101, (▽) 130, (*) 165, (○) 210, (+) 240 min.

salt concentration following a power-law, i.e., $W \approx [\mathrm{NaCl}]^{-c}$, with $c = 13.1$. This is similar to the value $c = 13.2$ for latexes at comparably high stability ratios found by Sefcik et al.[91]

4.1.2. Scaling and Master Curve for Aggregation Kinetics. On the basis of the developed aggregation model, as discussed in section 2.3, we expect to obtain aggregation master curves for the average radii as a function of τ, once the fractal dimension and the kernel parameter λ are fixed. We have shown above that $d_f = 1.8$ is constant for all the experimental conditions investigated. On the other hand, we can take also λ constant and equal to its average value $\lambda = 0.182$, if we neglect the scattered variations with ϕ_0 and [NaCl] shown in Figure 8a.

With this pair of d_f and λ values, we can compute the master curve for the average radii as a function of τ. If a master curve exists, we should then be able to scale all of the various experimental data considered above for the average radii on this master curve by selecting for each experiment a proper value of the stability ratio, W. This is indeed possible, as shown in Figure 9, and the obtained stability ratios are shown in Figure 8 (filled symbols). The agreement between the stability ratios estimated from the direct fitting of the experimental radii as a function of time and from master curve scaling is good, thus confirming the consistency of the developed analysis.

It is worth noting that the stability ratio values shown in Figure 8 indicate that the latex becomes more stable upon dilution with deionized water. The stability ratio W increases approximately by a factor of 3 when decreasing the solid volume fraction from $\phi_0 = 0.09$ to 0.05 at [NaCl] = 0.26 mol/L. This is probably due to the effect that dilution has on the pH as shown in Figure 1. As the latex is diluted, the *pH* increases thus promoting the dissociation of the surface carboxylic groups formed through reactions in eq 31 as discussed above. This leads to an increase of the particles surface charge and then to the observed increase of the stability ratio.[70,85]

4.1.3. Scaling and Master Curve for Gelation Kinetics. The gel formation kinetics for solid volume fractions $\phi_0 = 0.05$ and 0.09 and various salt concentrations has been investigated using in situ small strain oscillatory shear measurements. In particular, the elastic modulus $G'(\omega)$ has been monitored as a function of time at a frequency of $\omega = 100$ rad/s and a strain of $\gamma = 0.01\%$ as shown in Figure 10a. It is seen that the gelation time, defined as the measurable onset of a nonzero elasticity value, ranges from $t_g = 5$ min to 8 h (see inset in Figure 10a), depending on the experimental conditions. Following the results reported above on the aggregation master curve, also the elastic modulus data have been plotted as a function of the dimensionless time, τ in Figure 10b. To identify the possible existence of master curves also for gelation, the W values in the definition of the dimensionless time have been estimated in order to bring all of the G' curves together in two curves: one corresponding to $\phi_0 = 0.05$ and the other to 0.09. The obtained stability ratios are compared in Figure 8b with the ones obtained from the aggregation experiments and it is seen that they are in good agreement. This provides further support for the applicability of the kinetic aggregation model developed here up to the occurrence of gelation.

It is worth noting that for the gelation kinetics two different master curves are obtained for the two different values of the solid volume fraction. It is seen that the dimensionless gel time, τ_g depends on the solid volume fraction ϕ_0, and shorter

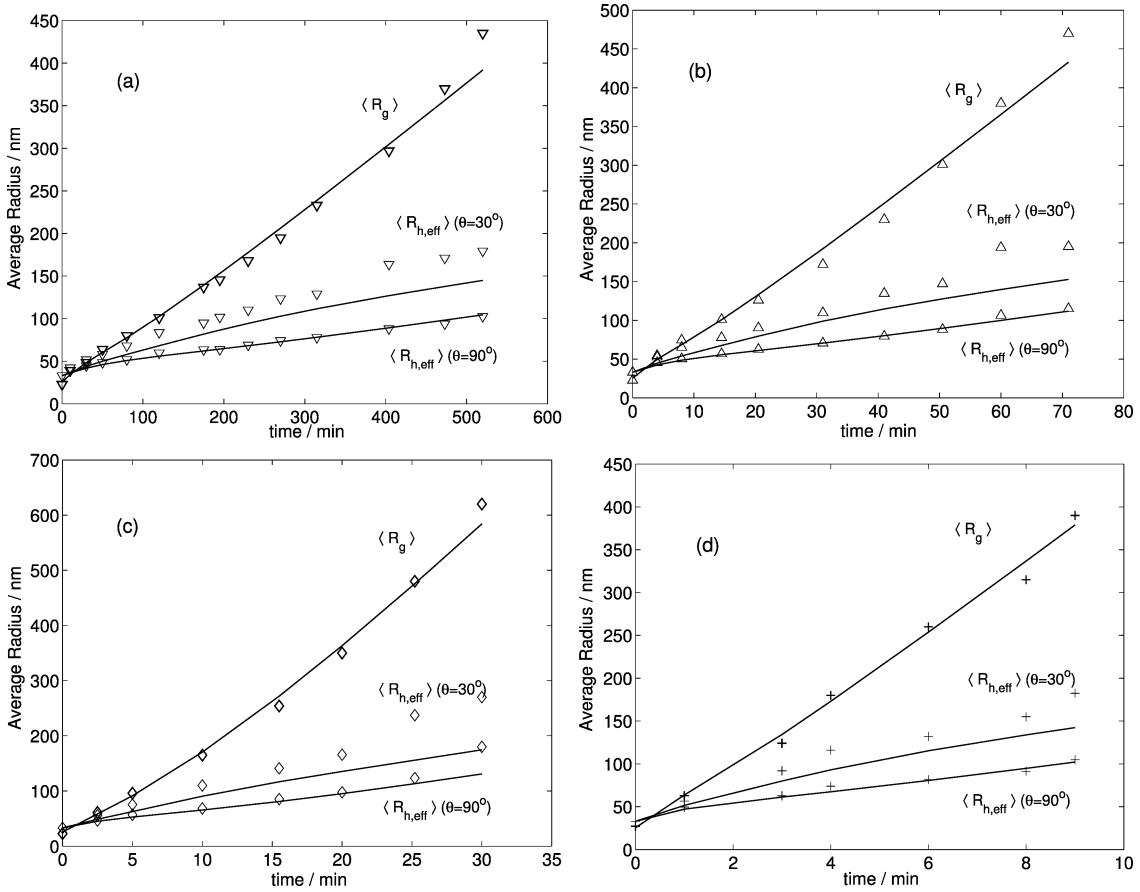

Figure 4. Comparison of the experimental (symbols) average radii as a function of time with the model calculations for $d_f = 1.8$ at $\phi_0 = 0.05$ and various salt concentrations. [NaCl] = (a) 0.24; (b) 0.28; (c) 0.30; (d) 0.32 mol/L.

dimensionless gel times are found for larger ϕ_0 values, but it is independent of the salt concentration or stability ratio.

This result is consistent with the observation above that the cumulative occupied volume fraction defined by eq 23, when expressed as a function of the dimensionless time, depends explicitly on ϕ_0 but not on W. This can be seen in Figure 11 where the values of the cumulative volume fractions, ϕ_x are shown as a function of the dimensionless time for the two solid volume fractions considered. It is seen that the occupied volume fractions at $\phi_0 = 0.09$ grow faster as a function of the dimensionless time than those at $\phi_0 = 0.05$. Since this growth represents the increase in the crowding of the system that eventually leads to gelation, it is reasonable to expect that the gelation point occurs earlier, as indeed indicated by the experimental data in Figure 10b.

4.2. Aggregation and Gelation Behavior of PS−SDS-Triton. In the following, we consider the aggregation behavior of the PS−SDS-Triton latex, which is the same PS−SDS latex considered above but further stabilized through the addition of the nonionic surfactant Triton X-100. The values of the average radii measured in two experimental runs at a salt concentration of [NaCl] = 0.5 mol/L and a solid volume fraction of $\phi_0 = 0.05$ are shown as a function of time in Figure 12a. The corresponding experimental structure factors are shown in Figure 12, parts b and c for various time values. Following the same fitting procedure described above, the following model parameter values have been found: $d_f = 1.75$, $\lambda = 0$ and $W = 1.75 \times 10^6$. From the comparison of the model results with the experimental data, shown in the same Figure 12, it can be seen that the agreement is again satisfactory although marginally worse than for the PS−SDS latexes.

It is worth noting that the value $W = 1.75 \times 10^6$ obtained above at $\phi_0 = 0.05$ and [NaCl] = 0.5 mol/L for the PS−SDS-Triton latex is similar to that exhibited by the PS−SDS latex at a lower salt concentration, i.e., [NaCl] = 0.26 mol/L (see Figure 8). Such a change in the salt concentration required to achieve an equivalent stability ratio is in good qualitative agreement with literature studies on the additional stabilizing effect of Triton X-100 on polystyrene colloids (although the polystyrene used therein is initially stabilized differently).[21−23]

The same experimental values of the average radii are compared in Figure 13 with the master curve computed with $d_f = 1.75$ and $\lambda = 0$. A comparison with the aggregation master curve of the PS−SDS latex in Figure 9 shows clearly that the addition of Triton has strongly changed the aggregation behavior of the system and specifically that the shape of the master curve is bending down compared to the bending up observed for PS−SDS.

This observation together with the value of $\lambda = 0$ indicates that this latex undergoes a slow RLCA process with a large stability ratio and an aggregation mechanism with a clear power-law growth typically found for DLCA.

The aggregation mechanisms of the two latexes are further compared in Figure 14 where the cumulative aggregate volume fractions are shown as a function of dimensionless time, τ. These calculations correspond to the conditions considered in Figures 9 and 13 and both are for a solid volume fraction of $\phi_0 = 0.05$. It is found that we can expect a larger dimensionless gelation time for the PS−SDS-Triton latex due to the slower crowding of the formed aggregates.

This is confirmed by the experimental values of the elastic modulus G' shown in Figure 15 for two repeated gelation

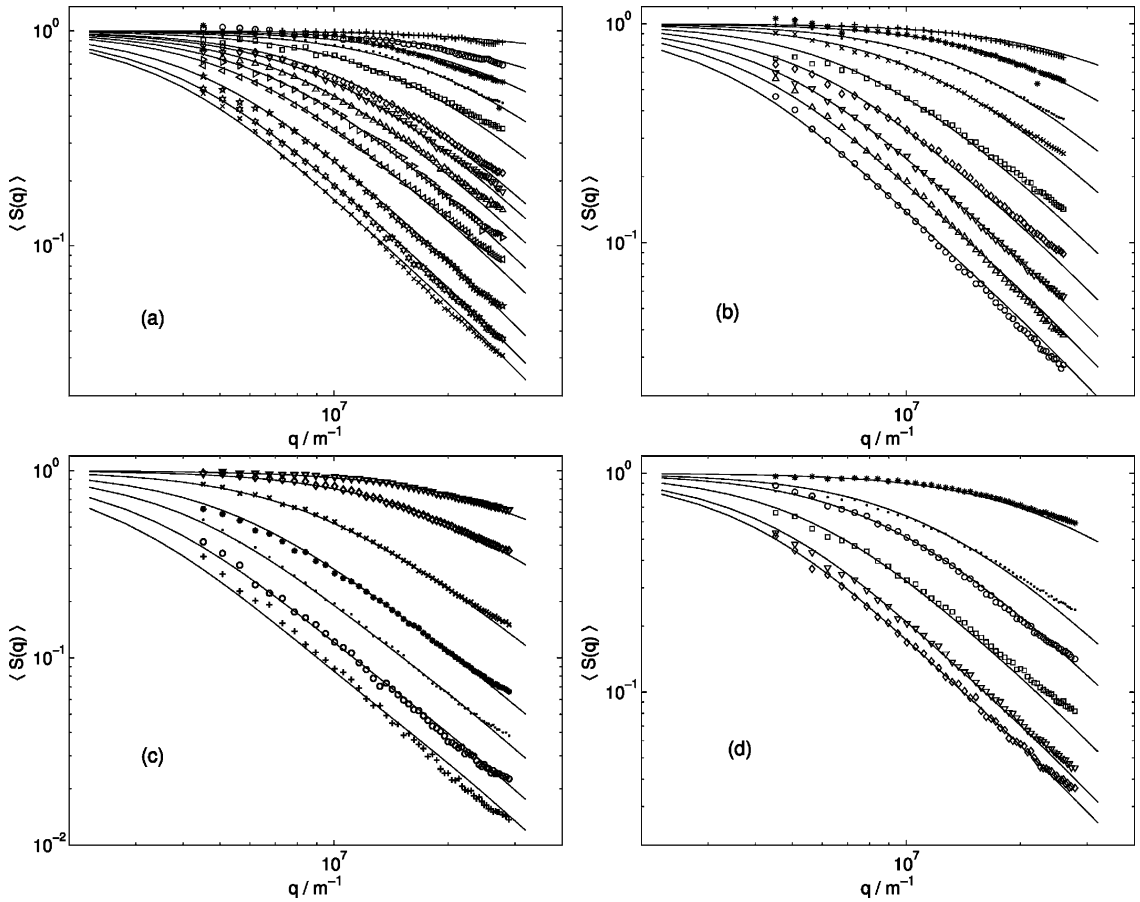

Figure 5. Comparison of the experimental (symbols) average structure factor as a function of q for various aggregation times with the model calculations for $d_f = 1.8$ at $\phi_0 = 0.05$ and various salt concentrations. [NaCl] = (a) 0.24; (b) 0.28; (c) 0.30; (d) 0.32 mol/L. Times increase from top to bottom and correspond to the $\langle R_g \rangle$ data shown in Figure 4a−d.

experiments conducted at the same operating conditions, i.e., [NaCl] = 0.5 mol/L and $\phi_0 = 0.05$, as a function of the dimensionless time τ. The same stability ratio $W = 1.75 \times 10^6$ obtained from the aggregation experiment has been used to scale the rheological data. Indeed, as expected, the dimensionless gelation time for the sample PS−SDS-Triton latex is significantly larger than the one found earlier for the PS−SDS latex.

4.3. Presence and Loss of Strain Hardening. The gels produced in the aggregation experiments described above have been further investigated by testing the frequency and strain dependence of the elastic modulus. The elastic and loss modulus of the gels exhibited no sensible frequency dependence and behaved as expected for elastic solids. The results were similar to the ones reported in Figure 1 of ref 43.

In Figure 16 are shown the elastic moduli normalized with respect to their approximated zero strain value as a function of the applied strain γ at a frequency of $\omega = 10$ rad/s, measured in an oscillatory shear experiment. The three independent gel samples prepared using the PS−SDS latex at [NaCl] = 0.28, 0.30, and 0.32 mol/L, are shown to exhibit strain hardening. This behavior was observed for all gels prepared from PS−SDS latexes. In the same figure are shown two measurements performed on the PS−SDS-Triton gels. Obviously, the additional adsorption of Triton X-100 on the polystyrene surface has changed the bonding force between the particles in the gel network, resulting in a different resistance to shear, including the loss of the strain hardening effect. This is confirmed by the different elastic moduli for the two systems, i.e., $G'(\gamma \rightarrow 0) =$ 2600 dyn/cm^2 for PS−SDS and 800 dyn/cm^2 for PS−SDS-Triton.

This latter finding can be explained by the effect of steric stabilization on the particle−particle separation distance within an aggregate or gel.[18−20,24−27] Particles stabilized by electrostatic forces as in the PS−SDS system aggregate in the deep primary minimum set by the attractive dispersion forces and thus exhibit a strong bond strength. A steric contribution in the form of an adsorbed or grafted nonionic surfactant prevents a close approach of the particle surfaces, and therefore leads to a weaker interparticle bond and to a smaller elastic modulus.

Justifying the loss of strain hardening is more complex. Strain hardening[43] is related to the properties of the gel backbone, its connectivity, and the strength of the bonds among primary particles. An applied strain stretches the contorted backbone of the gel and lengthens it. This results in an increased rigidity of the modified stress bearing path. This increased rigidity is measurable as an increased elastic modulus until the stretched bonds break and the gel collapses. If the bonds are weaker and do not resist bending and sliding as could be the case when steric layers are present on the particle surface, the network is less stiff and accommodates the stress by subtle rearrangement until the bonds are overstretched and break. Thus we could expect that both gels exhibit a comparable yield strain above which they both collapse, which might be somewhat larger for the PS−SDS-Triton latex due to easier accommodation of stresses through structural rearrangements. This is indeed observed in Figure 16. The surface modification with a nonionic surfactant therefore not only changes the aggregation behavior but also directly affects the final rheology of the gels formed at the end of the aggregation process. This underlines the importance of the interparticle interaction potential for the

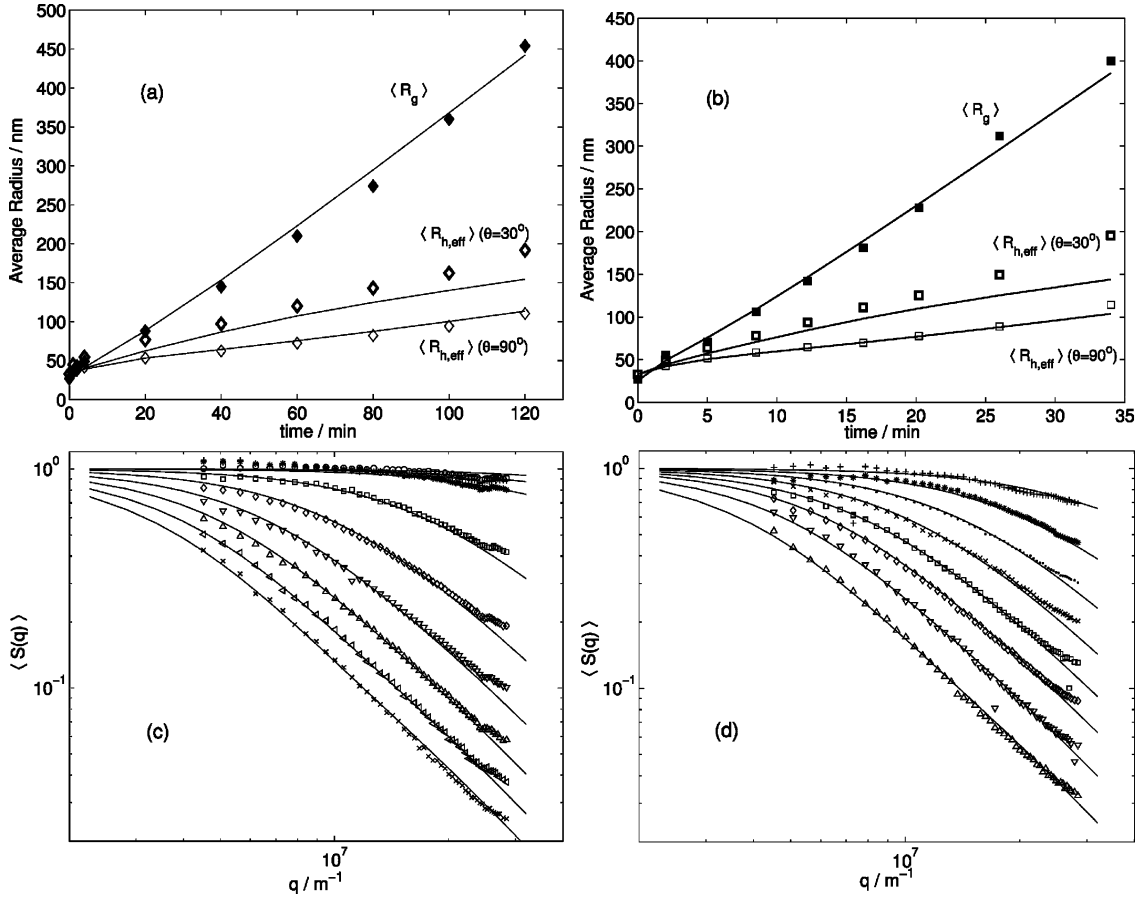

Figure 6. (a,b) Comparison of the experimental (symbols) average radii as a function of time with the model calculations for $d_f = 1.8$ at $\phi_0 = 0.09$ and two salt concentrations: [NaCl] = (a) 0.24; (b) 0.26 mol/L. (c,d) Comparison of the experimental (symbols) average structure factor as a function of q for various aggregation times with the model calculations for $d_f = 1.8$ at $\phi_0 = 0.09$ and two salt concentrations: (c) [NaCl] = 0.24; (d) 0.26 mol/L. Times in (c) and (d) increase from top to bottom and correspond to the $\langle R_g \rangle$ data shown in (a) and (b).

kinetics of the processes but also for the structure of the resulting aggregates and gels and for the related mechanical properties.

5. Discussion

5.1. Cluster Mass Distribution. The analysis reported above has shown that the model provides a good representation of the aggregation process in terms of the three different average radii of the CMD. This implies that the model reproduces not only the behavior of one average of the CMD but also of its polydispersity. The fact that the existence of an aggregation master curve, predicted by the model, has been verified experimentally further supports the model reliability. Considering the relatively large solid volume fractions investigated in this work, we should expect the presence of correlations among particles and clusters, which are often used as an argument against the applicability and validity of the PBE in eq 15. Although these correlations are definitely present, they do not influence the overall aggregation behavior at least in the conditions examined in this work. Three-body, or even many-body interactions have apparently no significant effect on the aggregation kinetics itself.

The probably most unexpected result is the existence of gelation master curves, based on the same dimensionless time used for the aggregation master curves, which implies that the developed kinetic aggregation model remains valid, at least in a certain effective sense, up to the gelation point, i.e., to conditions where the system is so crowded that the simple second-order aggregation kinetics would be expected to fail.

On the other hand, the experiments performed with the PS−SDS and PS−SDS-Triton latex indicate that the above conclusion and particularly the existence of kinetic master curves is subjected to the conditions of having constant surface chemistry. The introduction of a steric surfactant in the original latex drastically changed its aggregation behavior, reflected in the value of the kernel parameter λ.

5.2. Aggregate Structure and Aggregation Behavior. The analysis of the average aggregate structure factor in Figures 3, 5, 6, and 7 reveals that the aggregates formed at various salt concentrations and volume fractions exhibit a similar structure. The slope of the logarithm of the average structure factor as a function of the logarithm of q increases in time from values below unity to approximately 1.6−1.7, depending on when the last set of data for a particular run was taken. These data have been well reproduced by the developed model which uses a constant value of the fractal dimension and properly accounts for the polydispersity of the CMD evolving in time, and for the nonfractal behavior exhibited by the smaller aggregates. The latter is especially relevant in the investigated q vector range where the contribution of small aggregates is important.

The low fractal dimension $d_f = 1.8$ estimated by comparing model and experimental results is however surprising. In DLCA, a fractal dimension between $d_f = 1.7$ to 1.8 is expected to originate from the high reactivity of the clusters that aggregate upon every collision. This prevents the aggregates to interpenetrate significantly thus resulting in open structures. In RLCA the relatively small reactivity of clusters is expected to allow

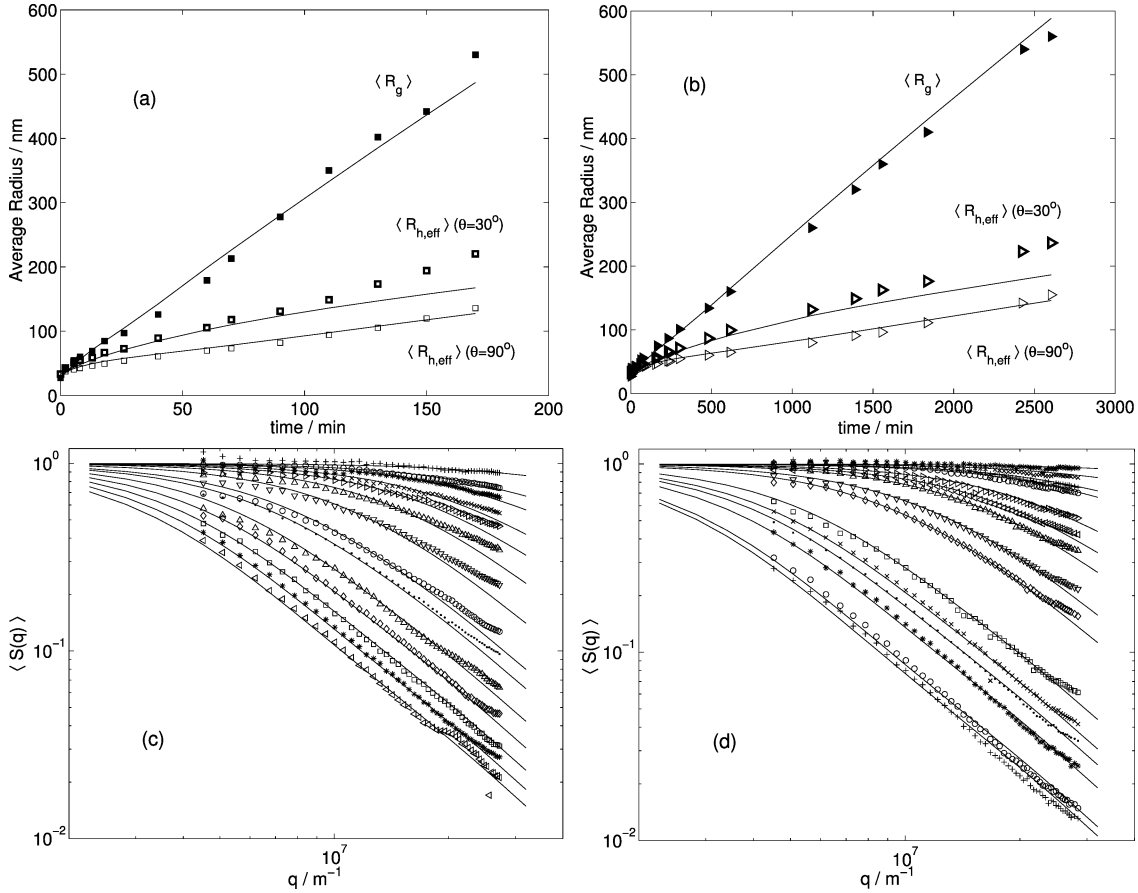

Figure 7. (a,b) Comparison of the experimental (symbols) average radii as a function of time with the model calculations for $d_f = 1.8$: (a) $\phi_0 = 0.01$, [NaCl] = 0.32 mol/L; (b) 0.005, 0.28 mol/L. (c,d) Comparison of the experimental (symbols) average structure factor as a function of q for various aggregation times with the model calculations for $d_f = 1.8$: (c) $\phi_0 = 0.01$, [NaCl] = 0.32 mol/L; (d) 0.005, 0.28 mol/L. Times in (c) and (d) increase from top to bottom and correspond to the $\langle R_g \rangle$ data shown in (a) and (b).

them to interpenetrate to a much larger extent than in DLCA thus resulting in larger fractal dimension such as $d_f = 2.1$. The aggregation process analyzed in this work is in the slow, RLCA-like regime, as it is clear from the large values of the stability ratio. However, the estimated value of the fractal dimension is 1.8, i.e., significantly smaller than the one expected in RLCA.

One possible explanation of this structural behavior is that aggregates of polymeric primary particles are rather flexible objects. This means that the exterior, extended parts of a reference aggregate, where interpenetration is supposed to take place, can be seen as excluded volumes for the branches of other aggregates in its proximity due to the strong relative movement of the branches of the reference aggregate. This wavy motion prevents other clusters from interpenetration and restricts the aggregation attempts to the outer surface of the clusters, resulting in relatively small fractal dimensions.

The parameter λ of the aggregation kernel characterizes how strongly the reactivity of an aggregate depends on its dimensionless mass i. In this work the product kernel expression $P_{ij} = (ij)^{\lambda}$ has been used to describe the reactivity dependence of the kernel on the mass i. This parameter λ is related for the product kernel by the simple relation $\lambda = \lambda_{DE}/2$ to the parameter λ_{DE} introduced by van Dongen and Ernst[53] in their classification of aggregation kernels. This relation allows to approximately connecting our kernel parameter λ to other results in the literature where the classification scheme of van Dongen and Ernst has been used.[15−19]

The PS−SDS and the PS−SDS-Triton latexes studied in this work exhibited, although aggregating in the slow RLCA regime, surprisingly small fractal dimensions equal to 1.8 and 1.75, and small kernel parameter values, i.e., $\lambda = 0.182$ and 0, respectively. In a previous work,[54] we have investigated the same PS−SDS latex but in the DLCA regime and found that the aggregate growth is characterized by the parameter values $\lambda = 0$ and $d_f = 1.7$, which are typical for DLCA.

For polystyrene colloids of various sizes in the DLCA regime, Tirado-Miranda et al.[15] showed that two bare polystyrene colloids with $R_p = 92$ and 121*nm* exhibited fractal dimensions and kernel parameters expected for DLCA, i.e., $\lambda_{DE} = 0.05$ with $d_f = 1.79$, and $\lambda_{DE} = 0.03$ with $d_f = 1.74$, respectively. On the other hand, a latex with a smaller radius, $R_p = 20$ nm, additionally stabilized with SDS, exhibited in DLCA a surprisingly large fractal dimension equal to 2.41, although λ_{DE} remained small and was equal to 0.06.

In a further study the same authors[19] investigated again polystyrene colloids of various sizes and confirmed for bare particles with $R_p = 120$ nm the DLCA regime with $\lambda_{DE} = 0.03$ and $d_f = 1.74$ and the RLCA regime with $\lambda_{DE} = 0.85$ and $d_f = 2.0$. Further results on an SDS stabilized polystyrene with $R_p = 20$ nm showed a decrease of the fractal dimension from 2.75 to 2.32 as a function of the increasing salt concentration. A fractal dimension typical of DLCA was however not observed, even at the highest salt concentrations. The values of the parameter λ_{DE} at high electrolyte concentrations were instead typical of DLCA, i.e., close to zero, whereas at lower electrolyte concentrations, a larger value of $\lambda = 0.6$ was found.

Another recent study[18] in dilute conditions ($\phi_0 \approx 8 \times 10^{-6}$) using bare polystyrene particles with $R_p = 50$ nm showed the expected decrease of the parameter λ_{DE} with increasing electrolyte concentration (thus changing from RLCA to DLCA). It

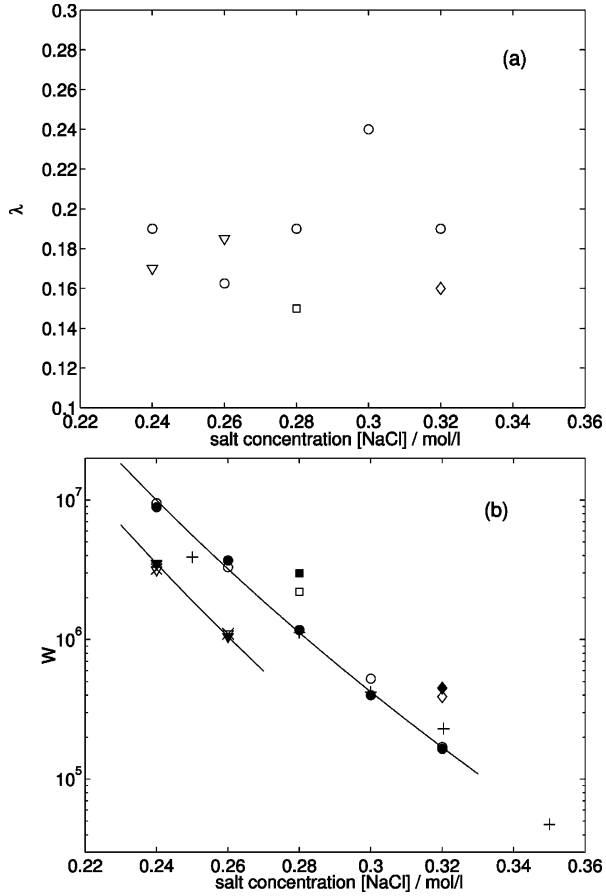

Figure 8. (a) Kernel parameter λ as a function of salt concentration obtained by fitting the experimental $\langle R_g \rangle$ values in Figures 2, 4, 6a,b, and 7a,b at various solid volume fractions: (○) $\phi_0 = 0.05$, (▽) 0.09, (◇) 0.01 (□) 0.005. (b) Stability ratio as a function of salt concentration at various solid volume fractions: (○) $\phi_0 = 0.05$, (▽) 0.09, (◇) 0.01 (□) 0.005, (−) power law fit, from fitting of the aggregation radii; (●) $\phi_0 = 0.05$, (▼) 0.09, (♦) 0.01 (■) 0.005, from the aggregation master curve scaling; (+) $\phi_0 = 0.05$, (×) 0.09, from the gelation master curve scaling.

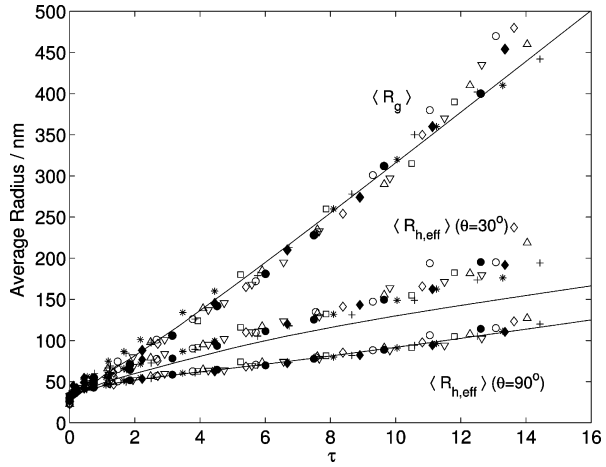

Figure 9. Aggregation master curve computed with $d_f = 1.8$ and $\lambda = 0.182$ compared with experimental data at various salt concentrations and solid volume fractions: (▽) [NaCl] = 0.24 mol/L, $\phi_0 = 0.05$; (△) 0.26, 0.05; (○) 0.28, 0.05; (◇) 0.30, 0.05; (□) 0.32, 0.05; (♦) 0.24, 0.09; (●) 0.26, 0.09; (+) 0.32, 0.01; (×) 0.28, 0.005. The stability ratios used are indicated by the solid symbols in Figure 8b.

is worth noting in this case that the slowest aggregation kinetics (RLCA) for bare polystyrene was characterized by $\lambda_{DE} \sim 0.5$, which corresponds to $\lambda \sim 0.25$, in good agreement with our

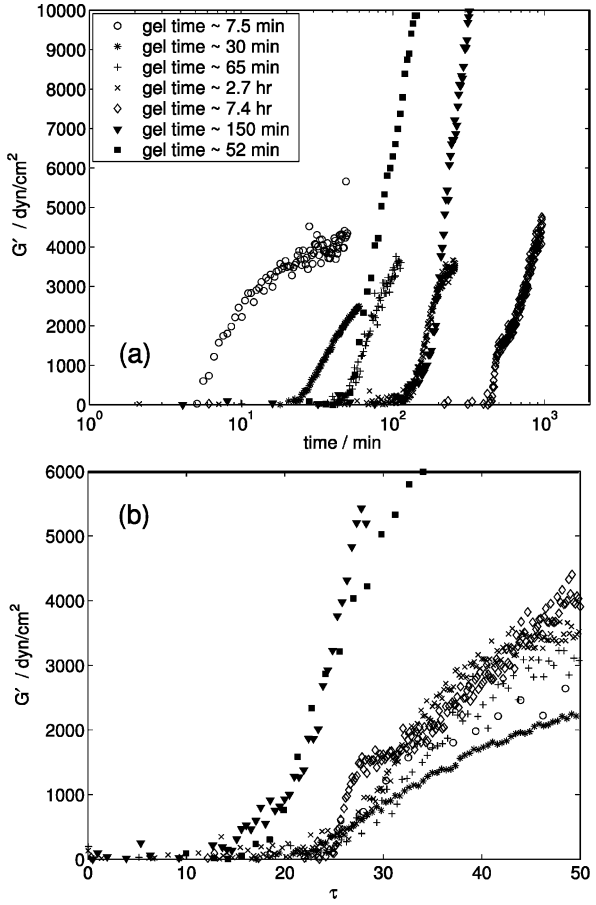

Figure 10. (a) Measured values of the elastic modulus as a function of (a) time and (b) dimensionless time for various values of the salt concentration and the solid volume fraction: (○) [NaCl] = 0.35 mol/L, $\phi_0 = 0.05$; (*) 0.32, 0.05; (+) 0.30, 0.05; (×) 0.28, 0.05; (◇) 0.25, 0.05; (▼) 0.24, 0.09; (■) 0.26, 0.09. The stability ratios used are indicated in Figure 8b.

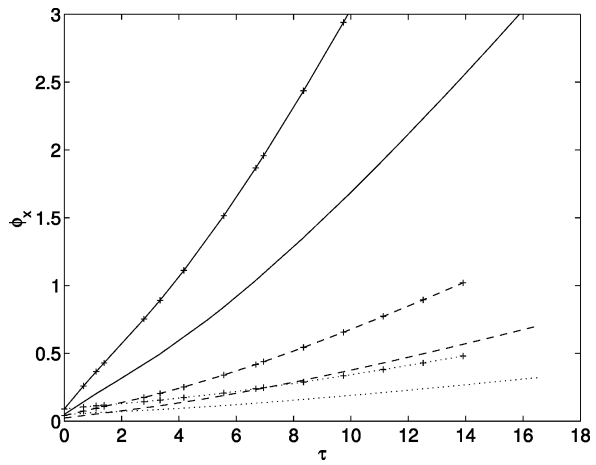

Figure 11. Comparison between the various calculated cumulative occupied volume fractions defined by eq 23 as a function of dimensionless time τ for two volume fractions: $\phi_0 = 0.05$: (−) ϕ_s; (- -) ϕ_g; (···) ϕ_h; and $\phi_0 = 0.09$: (− +) ϕ_s; (− − +) ϕ_g; (··· +) ϕ_h.

results at significantly higher solid volume fractions. In addition they investigated this polystyrene colloid at high electrolyte concentrations (DLCA) at various degrees of coverage with a protein at its isoelectric point and demonstrated a dependence of the parameter λ_{DE} on the degree of surface coverage. A similar effect has been studied in this work by adding Triton to the PS−SDS latex. It is remarkable that although in both cases nonionic macromolecules were used to change the particle

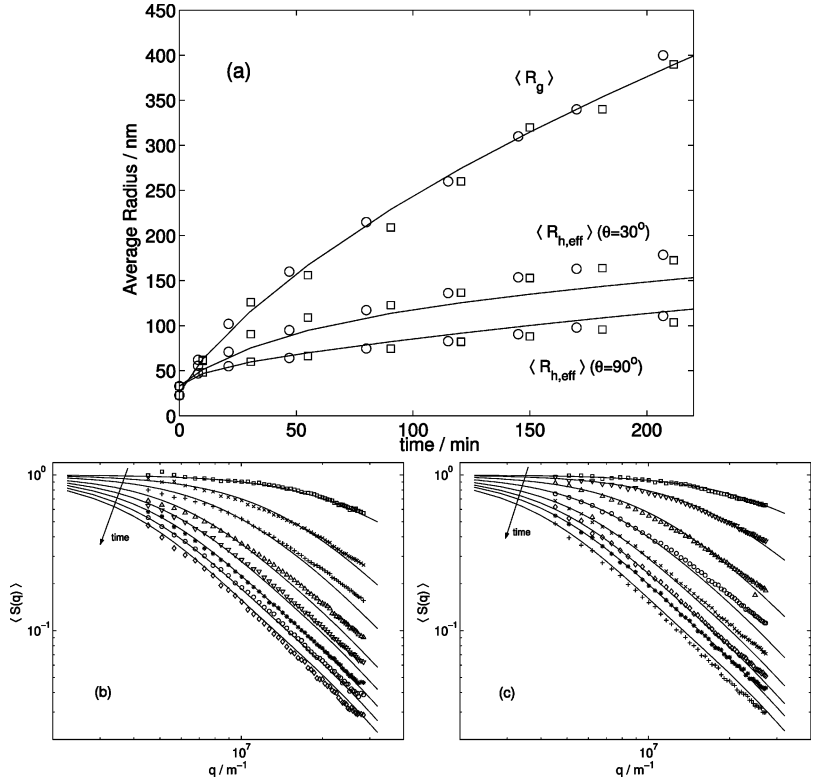

Figure 12. Comparison of the experimental (symbols) (a) average radii as a function of time and (b) and (c) the average structure factors as a function of q with the model calculations with $d_f = 1.75$, $W = 1.75 \times 10^6$ and $\lambda = 0$. PS−SDS-Triton latex at $\phi_0 = 0.05$ and [NaCl] = 0.5 mol/L. Times in (b) and (c) increase from top to bottom and correspond to the $\langle R_g \rangle$ data shown in (a): (□) for data in (b) and (○) for those in (c).

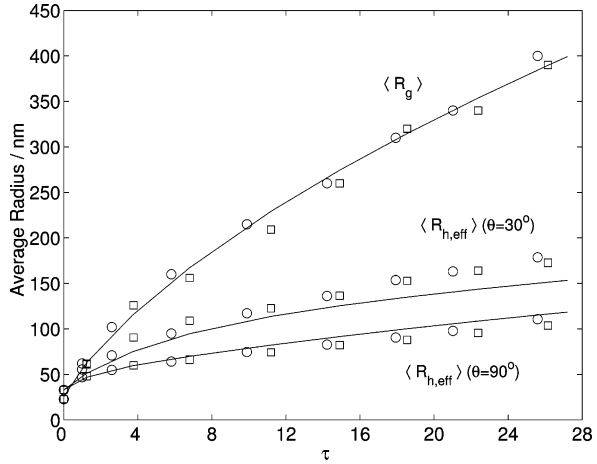

Figure 13. Master aggregation curve for the model calculations for $d_f = 1.75$ and $\lambda = 0$ and the experimental data in Figure 12 (symbols are the same).

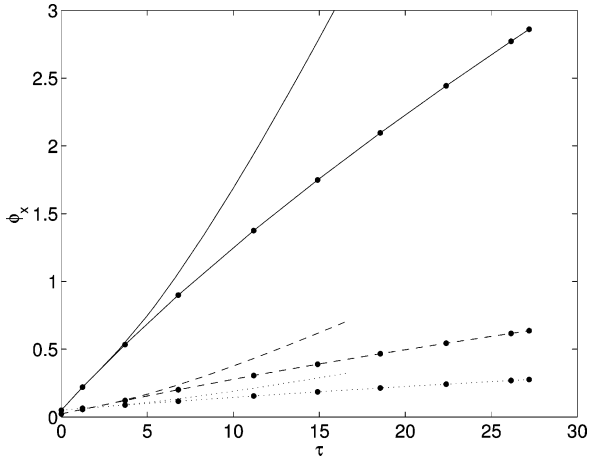

Figure 14. Comparison of calculated cumulative occupied volume fractions defined by eq 23 as a function of dimensionless time τ at $\phi_0 = 0.05$ for PS−SDS and PS−SDS-Triton latexes. PS−SDS: (−) ϕ_s; (− −) ϕ_g; (···) ϕ_h; PS−SDS-Triton: (− ●) ϕ_s; (− − ●) ϕ_g; (···●) ϕ_h.

interaction potential, an opposite effect on the value of λ was observed. In our case of high solid volume fractions in RLCA-type conditions a decrease of λ has been observed upon coverage of the particle surface with Triton X-100, whereas their study in DLCA-type conditions revealed an increase of λ with increasing coverage.

The results in these literature studies[15−19] in dilute conditions ($\phi_0 \approx 1 \times 10^{-5}$) together with our results at higher solid volume fractions indicate that the classical DLCA and RLCA regimes, with their characteristic rate of aggregation and aggregate structure, are only limiting conditions. In polymer latexes a larger variety of intermediate regimes are possible depending upon the particular surface chemistry and the respective preparation of the latex. More experiments are needed in order to understand this complex interplay among the surface chemistry of the aggregating particles, their kinetic aggregation behavior (λ) and their structure (d_f), at different solid volume fractions.

6. Conclusions

In this work we developed a model based on PBE in dimensionless form for the aggregation of colloidal dispersions in nonsheared conditions. We reported a set of data at relatively large solid volume fractions ($\phi_0 < 0.1$), well characterized in terms of various moments of the CMD measured by light scattering, i.e., the gyration and hydrodynamic radii and the average structure factor, and rheological measurements, where the gelation point has been estimated as the point of onset of a nonzero elastic modulus. The good agreement of the experi-

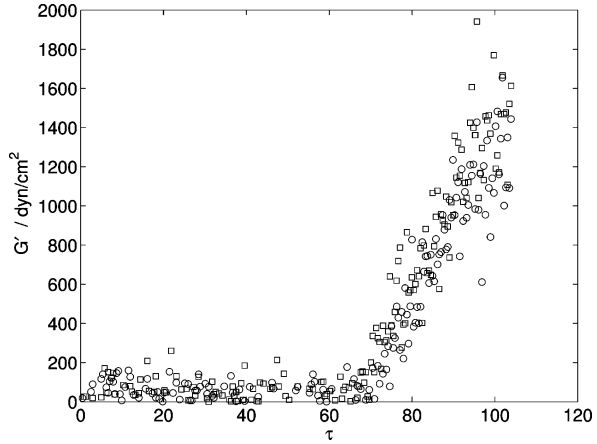

Figure 15. Elastic modulus values as a function of dimensionless time τ for a PS−SDS-Triton latex at $\phi_0 = 0.05$ and [NaCl] = 0.5 mol/L. The stability ratio is the same as in the aggregation master curve in Figure 12, i.e., $W = 1.75 \times 10^6$. (□) and (○) correspond to two repeated experiments.

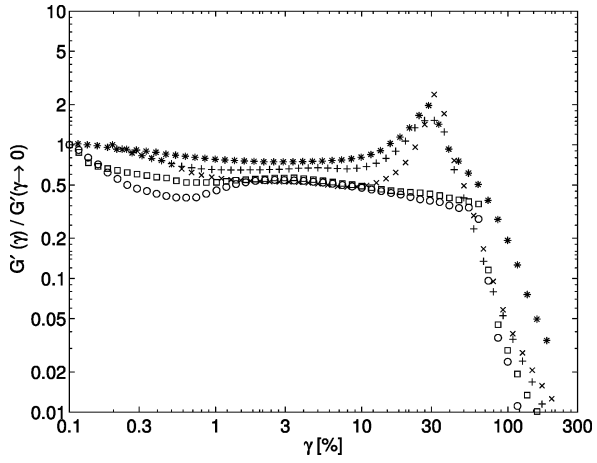

Figure 16. Normalized elastic modulus $G'(\gamma)/G'(\gamma \rightarrow 0)$ as a function of strain, γ for PS−SDS gels ((*),(×),(+)) at [NaCl] = 0.28, 0.30, and 0.32 mol/L and PS−SDS-Triton ((□),(○)) at [NaCl] = 0.5 mol/L. The average elastic modulus is $G'(\gamma \rightarrow 0) = 2605$ dyn/cm^2 for PS−SDS and 800 dyn/cm^2 for PS−SDS-Triton.

mental and model results prove the existence of an aggregation master curve that describes the average radii as a function of the dimensionless time, τ for various W and ϕ_0 values, as long as λ and d_f, which are the parameters describing the aggregation kernel and the aggregate structure, are constant. In addition to the aggregation master curve it is found that using the same dimensionless time a normalized curve is obtained also for the gelation kinetics. This indicates that, at least for the examined conditions, the developed model based on PBE can be extended up to the formation of a gel phase. Further experimental runs conducted with a differently stabilized polystyrene latex indicated that surface chemistry plays a fundamental role in determining not only the stability ratio, W but also the aggregation kinetics through the value of λ as well as the intrinsic structure of the aggregates. This is for example demonstrated by the disappearance of the strain hardening effect upon addition of a further steric stabilization of the polymer latex.

Acknowledgment. We thank Sven Ritschard for performing some of the rheological measurements and Marco Lattuada, Hua Wu, and Andrea Vaccaro for many discussions. Fruitful comments and ideas raised in discussions with Peter Schurtenberger and Frank Scheffold are gratefully acknowledged. This work was performed with financial support by the Swiss National Science Foundation (NSF), under Grant No. 2000-061883.

Notation

Roman Capital Letters

B_{ij} = part of matrix of aggregation rate constant
D_i = diffusion coefficient for aggregates of mass i
$D_{i,\mathrm{eff}}$ = effective diffusion coefficient for aggregates of mass i
D_0 = diffusion coefficient of primary particle
$\langle D_{\mathrm{eff}} \rangle$ = effective diffusion coefficient of population of aggregates
F_i = function in the pair correlation function model
$\mathscr{T}_{g,i}$ = dimensionless pair-correlation function
G' = elastic modulus
G'' = loss modulus
$I(q)$ = intensity of scattered light
K_B = Brownian aggregation rate constant
K_{ij} = matrix of aggregation rate constants
K_{11} = primary particle aggregation rate constants
M_w = average molecular weight
N_i = number density of aggregates and particles
$N_i^{nn} = g(r)$ parameter
N_0 = initial number of primary particles per unit volume
P_{ij} = part of matrix of aggregation rate constant
$P(q)$ = primary particle form factor
$Q = qR_p$ = dimensionless scattering wave vector
$R_{g,i}$ = radius of gyration of mass i
$R_{h,i}$ = hydrodynamic radius of mass i
$R_{c,i}$ = collision radius of mass i
$R_{h,r,i}$ = rotational hydrodynamic radius of mass i
R_p = primary particle radius
$R_{p,g}$ = primary particle radius of gyration
$S_i(q)$ = dimensionless aggregate structure factor, eq 6
$\langle S_i(q) \rangle$ = dimensionless average structure factor, eq 17
T = absolute temperature
W = stability ratio
X_i = dimensionless number density

Roman Letters

$a_i = g(r)$ model parameter
$b_i = g(r)$ model parameter
$c_i = g(r)$ model parameter
$d = g(r)$ model parameter
d_f = fractal scaling exponent (fractal dimension)
$e = g(r)$ model parameter
$f = g(r)$ model parameter
$f(q, t)$ = dynamic structure factor
$g_T^{(2)}(q, t)$ = time averaged autocorrelation function
$g(r)$ = pair correlation function
$l = g(r)$ model parameter
i = dimensionless aggregate mass
k_B = Boltzmann constant
k_f = prefactor in fractal scaling relation (hydrodynamic properties)
$m = g(r)$ model parameter
n = liquid refractive index
q = scattering wave vector
r = length scale inside fractal aggregates
s = dimensionless distance $s = r/R_p$
t = time

t_g = gelation time

Greek Capital Letters

Γ_1 = first cumulant of correlation function
Γ_2 = second cumulant of correlation function
Γ_3 = third cumulant of correlation function
$\Gamma(x)$ = gamma function
$\Gamma_{inc}(x)$ = incomplete gamma function
$\Omega_{h,i,eff}$ = dimensionless effective hydrodynamic radius

Greek Letters

β_i = ratio of hydrodynamic and gyration radii
γ_i = pair correlation function parameter-exponent
γ = strain in rheology
$\delta(x)$ = delta function
η = solvent dynamic viscosity
θ = scattering angle
λ = aggregation kernel exponent
λ_0 = wavelength of light
λ_{DE} = van Dongen/Ernst homogeneity kernel parameter[53]
ξ_i = pair correlation function parameter-cutoff size
ξ_i^* = dimensionless cutoff size
π = constant
ρ_p = density of polymer
ρ_l = density of liquid phase
ρ_h = dimensionless hydrodynamic radius
ρ_g = dimensionless radius of gyration
ρ_c = dimensionless collision radius
τ = dimensionless time
ϕ_0 = solid volume fraction
ϕ_x = cumulative volume fraction (indices *g*, *h*, *c*)
ω = frequency

Indices

i, *j*, *k* = counter, indexing mass

Special Symbols

$\langle\rangle$ = ensemble or time average
[NaCl] = sodium chloride concentration
PS−SDS = polystyrene stabilized with SDS
PS−SDS−Triton = polystyrene stabilized with SDS and Triton-X100
pH = logarithm of proton activity
SDS = sodium dodecyl sulfate ($C_{12}H_{25}SO_4Na$)
rms = root-mean-square error

References and Notes

(1) Lin, M.; Lindsay, H.; Weitz, D.; Ball, R.; Klein, R.; Meakin, P. Universality in colloid aggregation. *Nature* **1989**, *339*, 360.

(2) Lin, M.; Lindsay, H.; Weitz, D.; Klein, R.; Ball, R.; Meakin, P. Universal Reaction-Limited Aggregation. *Phys. Rev. A* **1990**, *41*, 2005.

(3) Lin, M.; Lindsay, H.; Weitz, D.; Ball, R.; Klein, R.; Meakin, P. Universal Diffusion-Limited Aggregation. *J. Phys.: Condens. Matter* **1990**, *2*, 3093.

(4) Carpineti, M.; Ferri, F.; Giglio, M.; Paganini, E.; Perini, U. Salt-induced fast aggregation of polystyrene latex. *Phys. Rev. A* **1990**, *42*, 7347.

(5) Asnaghi, D.; Carpineti, M.; Giglio, M.; Sozzi, M. Coagulation kinetics and aggregate morphology in the intermediate regimes between diffusion-limited and reaction-limited cluster aggregation. *Phys. Rev. A* **1992**, *45*, 1018.

(6) Carpineti, M.; Giglio, M. Spinodal-type dynamics in fractal aggregation of colloidal clusters. *Phys. Rev. Lett.* **1992**, *68*, 3327.

(7) Carpineti, M.; Giglio, M. Transition from semiorder to disorder in the aggregation of dense colloidal solutions. *Phys. Rev. Lett.* **1993**, *70*, 3828.

(8) Sciortino, F.; Tartaglia, P. Structure Factor Scaling during Irreversible Cluster-Cluster Aggregation. *Phys. Rev. Lett.* **1995**, *74*, 282.

(9) Sciortino, F.; Belloni, A.; Tartaglia, P. Irreversible diffusion-limited cluster aggregation: the behavior of the scattered intensity. *Phys. Rev. E* **1995**, *52*, 4068.

(10) Odriozola, G.; Schmitt, A.; Callejas-Fernandez, J.; Martinez-Garcia, R.; Hidalgo-Alvarez, R. Dynamic Scaling Concepts Applied to Numerical Solutions of Smoluchowski's Rate Equation. *J. Chem. Phys.* **1999**, *111*, 7657.

(11) Odriozola, G.; Moncho-Jorda, A.; Schmitt, A.; Callejas-Fernandez, J.; Martinez-Garcia, R.; Hidalgo-Alvarez, R. A Probabilistic Aggregation Kernel for the Computer-Simulated Transition from DLCA to RLCA. *Europhys. Lett.* **2001**, *53*, 797.

(12) Moncho-Jorda, A.; Odriozola, G.; Martinez-Lopez, F.; Schmitt, A.; Hidalgo-Alvarez, R. The DLCA-RLCA transition arising in 2D-aggregation: simulations and mean field theory. *Eur. Phys. J. E* **2001**, *5*, 471.

(13) Hanus, L.; Hartzler, R.; Wagner, N. Electrolyte-Induced Aggregation of Acrylic Latex. 1. Dilute Particle Concentrations. *Langmuir* **2001**, *17*, 3136.

(14) Leone, R.; Odriozola, G.; Mussio, L.; Schmitt, A.; Hidalgo-Alvarez, R. Coupled Aggregation and Sedimentation processes: Three-dimensional off-lattice simulations. *Eur. Phys. J. E* **2003**, *7*, 153.

(15) Tirado-Miranda, M.; Schmitt, A.; Callejas-Fernandez, J.; Fernandez-Barbero, A. Test of the Physical Interpretation of the structural coefficient for colloidal clusters. *Langmuir* **2000**, *16*, 7541.

(16) Tirado-Miranda, M.; Schmitt, A.; Callejas-Fernandez, J.; Fernandez-Barbero, A. Aggregation of protein-coated colloidal particles: Interaction energy, cluster morphology, and aggregation kinetics. *J. Chem. Phys.* **2003**, *119*, 9251.

(17) Tirado-Miranda, M.; Schmitt, A.; Callejas-Fernandez, J.; Fernandez-Barbero, A. The aggregation behavior of protein-coated colloidal particles: a light scattering study. *Eur. Biophys. J.* **2003**, *32*, 128.

(18) Tirado-Miranda, M.; Schmitt, A.; Callejas-Fernandez, J.; Fernandez-Barbero, A. Clustering under short-range finite interactions. *Phys. Rev. E* **2003**, *67*, 011402.

(19) Tirado-Miranda, M.; Schmitt, A.; Callejas-Fernandez, J.; Fernandez-Barbero, A. Colloidal clusters with finite binding energies: Fractal structure and growth mechanism. *Langmuir* **1999**, *15*, 3437.

(20) Liu, J.; Shih, W.; Sarikaya, M.; Aksay, I. Fractal colloidal aggregates with finite interparticle interactions: energy dependence of the fractal dimension. *Phys. Rev. A* **1990**, *41*, 3206.

(21) Romero-Cano, M.; Martin-Rodriguez, A.; Chauveteau, G.; de las Nieves, F. Colloidal Stabilization of Polystyrene Particles by Adsorption of Nonionic Surfactants II. Electrosteric Stability Studies. *J. Colloid Interface Sci.* **1998**, *198*, 273.

(22) Romero-Cano, M.; Martin-Rodriguez, A.; de las Nieves, F. Electrosteric Stabilization of Polymer Colloids with Different Functionality. *Langmuir* **2001**, *17*, 3505.

(23) Porcel, R.; Jodar, A.; Cabrerizo, A.; Hidalgo-Alvarez, R.; Martin-Rodriguez, A. Sequential Adsorption of Triton X-100 and Sodium Dodecyl Sulfate onto Positively and Negatively Charged Polystyrene Latexes. *J. Colloid Interface Sci.* **2001**, *239*, 568.

(24) de Rooij, R.; van den Ende, D.; Duits, M.; Mellema, J. Elasticity of weakly aggregating polystyrene latex dispersions. *Phys. Rev. E* **1994**, *49*, 3038.

(25) Goodwin, J.; Hughes, R.; Partridge, S.; Zukoski, C. The elasticity of weakly flocculated suspensions. *J. Chem. Phys.* **1986**, *85*, 559.

(26) Potanin, A.; de Rooij, R.; van den Ende, D.; Mellema, J. Microrheological modeling of weakly aggregated dispersions. *J. Chem. Phys.* **1995**, *102*, 5845.

(27) de Rooij, R.; Potanin, A.; van den Ende, D.; Mellema, J. Steady shear viscosity of weakly aggregating polystyrene latex dispersions. *J. Chem. Phys.* **1993**, *99*, 9213.

(28) Buscall, R.; Mills, P.; Yates, G. Viscoelastic Properties of Strongly-Flocculated Polystyrene Latex Suspensions. *Colloids and Surfaces* **1986**, *18*, 341.

(29) Buscall, R.; McGowan, I.; Mills, P.; Stewart, R.; Sutton, D.; White, L.; Yates, G. The Rheology of Strongly-Flocculated Suspensions. *J. Non-Newtonian Fluid Mechan.* **1987**, *24*, 183.

(30) Wyss, H.; Romer, S.; Scheffold, F.; Schurtenberger, P.; Gauckler, L. Diffusing-Wave Spectroscopy of Concentrated Alumina Suspensions during Gelation. *J. Colloid Interface Sci.* **2001**, *240*, 89.

(31) Romer, S.; Scheffold, F.; Schurtenberger, P. Sol−Gel Transition of Concentrated Colloidal Suspensions. *Phys. Rev. Lett.* **2000**, *85*, 4980.

(32) Bergenholtz, J.; Fuchs, M. Nonergodicity transitions in colloidal suspensions with attractive interactions. *Phys. Rev. E* **1999**, *59*, 5706.

(33) Bergenholtz, J.; Fuchs, M.; Voigtmann, T. Colloidal gelation and nonergodicity transitions. *J. Phys.: Condens. Matter* **2000**, *12*, 6575.

(34) Puertas, A.; Fuchs, M.; Cates, M. Comparative Simulation Study of Colloidal Gels and Glasses. *Phys. Rev. Lett.* **2001**, *88*, 098301.

(35) Kroy, K.; Cates, M.; Poon, W. Cluster mode-coupling approach to weak gelation in attractive colloids. *Phys. Rev. Lett.* **2004**, *92*, 148302.

(36) Bergenholtz, J.; Poon, W.; Fuchs, M. Gelation in model colloid-polymer mixtures. *Langmuir* **2003**, *19*, 4493.

(37) Martin, J.; Wilcoxon, J. Critical Dynamics of the Sol−Gel Transition. *Phys. Rev. Lett.* **1988**, *61*, 373.

(38) Martin, J.; Wilcoxon, J.; Odinek, J. Decay of density fluctuations in gels. *Phys. Rev. A* **1991**, *43*, 858.

(39) Segre, P.; Prasad, V.; Schofield, A. B.; Weitz, D. A. Glasslike Kinetic Arrest near the Colloidal-Gelation Transition. *Phys. Rev. Lett.* **2001**, *86*, 6042.

(40) Nicolai, T.; Cocard, S. Structure of gels and aggregates of disklike colloids. *Eur. Phys. J. E* **2001**, *5*, 221.

(41) Nicolai, T.; Cocard, S. Dynamic Light-Scattering Study of Aggregating and Gelling Colloidal Disks. *J. Colloid Interface Sci.* **2001**, *244*, 51.

(42) Krall, A.; Huang, Z.; Weitz, D. Dynamics of Density Fluctuations in Colloidal Gels. *Physica A* **1997**, *235*, 19.

(43) Gisler, T.; Ball, R.; Weitz, D. Strain Hardening of Fractal Colloidal Gels. *Phys. Rev. Lett.* **1999**, *82*, 1064.

(44) Le Bon, C.; Nicolai, T.; Durand, D. Kinetics of Aggregation and Gelation of Globular Proteins after Heat-Induced Denaturation. *Macromolecules* **1999**, *32*, 6120.

(45) Weijers, M.; Visschers, R.; Nicolai, T. Light Scattering Study of Heat-Induced Aggregation and Gelation of Ovalbumin. *Macromolecules* **2002**, *35*, 4753.

(46) Dixit, N.; Zukoski, C. Competition between crystallization and gelation: A local description. *Phys. Rev. E* **2003**, *67*, 061501.

(47) Kulkarni, A.; Dixit, N.; Zukoski, C. Ergodic and nonergodic phase transitions in globular protein suspensions. *Faraday Discuss.* **2003**, *123*, 37−50.

(48) Gimel, J.; Durand, D.; Nicolai, T. Transition between flocculation and percolation of a diffusion-limited cluster−cluster aggregation process using three-dimensional Monte Carlo simulation. *Phys. Rev. B* **1995**, *51*, 11348.

(49) Gimel, J.; Durand, D.; Nicolai, T. 3D Monte Carlo Simulations of Diffusion-Limited Cluster Aggregation up to the Sol−Gel Transition: Structure and Kinetics. *J. Sol-Gel Sci. Technol.* **1999**, *15*, 129.

(50) Prasad, V.; Trappe, V.; Dinsmore, A.; Segre, P.; Cipelletti, L.; Weitz, D. Universal Features of the fluid to solid transition for attractive colloidal particles. *Faraday Discuss.* **2003**, *123*, 1.

(51) Elliot, S.; Butera, R.; Hanus, L.; Wagner, N. Fundamentals of aggregation in concentrated dispersions: Fiber-optic quasielastic light scattering and linear viscoelastic measurements. *Faraday Discuss.* **2003**, *123*, 369.

(52) van Dongen, P.; Ernst, M. Cluster Size Distribution in Irreversible Aggregation at Large Times. *J. Phys. A: Math. Gen.* **1985**, *18*, 2779.

(53) van Dongen, P.; Ernst, M. Dynamic Scaling in the Kinetics of Clustering. *Phys. Rev. Lett.* **1985**, *54*, 1396.

(54) Sandkühler, P.; Sefcik, J.; Morbidelli, M. Kinetics of gel formation in dilute dispersions with strong attractive particle interactions. *Adv. Colloid and Interface Sci.* **2004**, *108*−*109*, 133−143.

(55) Larson, R. *The Structure and Rheology of Complex Fluids*; Oxford University Press: New York, 1999.

(56) Dickinson, E.; Bergenstahl, B. e. *Food Colloids*; The Royal Society of Chemistry: London, 1997.

(57) Brinker, C.; Scherer, G. *Sol*−*Gel Science*; Academic Press: San Diego, CA, 1990.

(58) Trappe, V.; Sandkühler, P. Colloidal gels − low-density disordered solidlike states. *Curr. Opin. Colloid Interface Sci.* **2004**, *8*, 494−500.

(59) Lattuada, M.; Sandkühler, P.; Wu, H.; Sefcik, J.; Morbidelli, M. Aggregation kinetics of polymer colloids in reaction limited regime: Experiments and simulations. *Adv. Colloid Interface Sci.* **2003**, *103*, 33.

(60) Lattuada, M.; Wu, H.; Sandkühler, P.; Sefcik, J.; Morbidelli, M. Modelling of aggregation kinetics of colloidal systems and its validation by light scattering measurements. *Chem. Eng. Sci.* **2004**, *59*, 1783.

(61) Lattuada, M.; Sandkühler, P.; Wu, H.; Sefcik, J.; Morbidelli, M. Kinetic Modeling of Aggregation and Gel Formation in Quiescent Dispersions of Polymer Colloids. *Macromol. Symp.* **2004**, *206*, 307−320.

(62) Lattuada, M.; Wu, H.; Hasmy, A.; Morbidelli, M. Estimation of Fractal Dimension in Colloidal Gels. *Langmuir* **2003**, *19*, 6312−6316.

(63) Lattuada, M.; Wu, H.; Morbidelli, M. A Simple Model for the Structure of Fractal Aggregates. *J. Colloid Interface Sci.* **2003**, *268*, 106−120.

(64) Lattuada, M.; Wu, H.; Morbidelli, M. Hydrodynamic radius of fractal clusters. *J. Colloid Interface Sci.* **2003**, *268*, 96−105.

(65) Lattuada, M.; Wu, H.; Morbidelli, M. Rotational diffusivity of fractal clusters. *Langmuir* **2004**, *20*, 5630−5636.

(66) Lattuada, M.; Wu, H.; Morbidelli, M. Radial density distribution of fractal clusters. *Chem. Eng. Sci.* **2004**, in press.

(67) Kirkwood, J.; Riseman, J. The intrinsic viscosities and diffusion constants of flexible macromolecules in solution. *J. Chem. Phys.* **1948**, *16*, 565.

(68) Sandkühler, P.; Sefcik, J.; Lattuada, M.; Wu, H.; Morbidelli, M. Modeling Structure Effects on Aggregation Kinetics in Colloidal Dispersions. *AIChE J.* **2003**, *49*, 1542.

(69) Spielman, L. Viscous Interactions in Brownian Coagulation. *J. Colloid Interface Sci.* **1970**, *33*, 562.

(70) Behrens, S.; Christl, D.; Emmerzael, R.; Schurtenberger, P.; Borkovec, M. Charging and Aggregation Properties of Carboxyl Latex Particles: Experiments versus DLVO Theory. *Langmuir* **2000**, *16*, 2566.

(71) Family, F.; Meakin, P.; Vicsek, T. Cluster Size Distribution in Chemically Controlled Cluster-Cluster Aggregation. *J. Chem. Phys.* **1985**, *83*, 4144.

(72) Zhu, P.; Napper, D. Studies of aggregation kinetics of polystyrene latices sterically stabilized by poly(N-isopropylacrylamide). *Phys. Rev. E* **1994**, *50*, 1360−1366.

(73) Dinsmore, A.; Weitz, D. Direct imaging of three-dimensional structure and topology of colloidal gels. *J. Phys.: Condens Matter* **2002**, *14*, 7581−7597.

(74) Anderson, V.; de Hoog, E.; Lekkerkerker, H. Mechanisms of phase separation and aggregation in colloid-polymer mixtures. *Phys. Rev. E* **2002**, *65*, 011403.

(75) Sandkühler, P.; Lattuada, M.; Wu, H.; Sefcik, J.; Morbidelli, M. Further Insights into the Universality of Colloid Aggregation. *Adv. Colloid Interface Sci.* **2004**, submitted.

(76) Lindsay, H.; Lin, M.; Weitz, D.; Ball, R.; Klein, R.; Meakin, P. Light Scattering from Fractal Colloid Aggregates. In *OSA Proceedings on Photon Correlation Techniques and Applications*, Vol. 1; Abbiss, J.; Smart, A., Eds.; Optical Society of America: Washinghton, DC, 1988; p 122.

(77) Lin, M.; Lindsay, H.; Weitz, D.; Ball, R.; Klein, R.; Meakin, P. Universality of fractal aggregates as probed by light scattering. *Proc. R. Soc. London A* **1989**, *423*, 71.

(78) Torres, F.; Russel, W.; Schowalter, W. Floc Structure and Growth Kinetics for Rapid Shear Coagulation of Polystyrene Colloids. *J. Colloid Interface Sci.* **1991**, *142*, 554.

(79) Linder, P.; Zemb, T. *Neutrons, X-rays and Light: Scattering Methods Applied to Soft Condensed Matter*; Elsevier Science B. V.: Amsterdam, The Netherlands, 2002.

(80) Berne, B.; Pecora, R. *Dynamic Light Scattering*; Wiley: New York, 1976.

(81) Degiorgio, V.; Piazza, R.; Bellini, T.; Visca, M. Static and Dynamic Light Scattering Study of Fluorinated Polymer Colloids with a Crystalline Internal Structure. *Adv. Colloid Interface Sci.* **1994**, *48*, 61.

(82) Higgins, J.; Benoit, H. *Polymers and Neutron Scattering*; Oxford Science Publications: New York, 1994.

(83) Pusey, P.; van Megen, W. Dynamic Light Scattering by Non-Ergodic Media. *Physica A* **1989**, *157*, 705.

(84) Gilbert, R. *Emulsion Polymerization: A Mechanistic Approach*; Academic Press: London, 1995.

(85) Sefcik, J.; Verduyn, M.; Storti, G.; Morbidelli, M. Charging of Latex Particles Stabilized by Sulfate Surfactant. *Langmuir* **2003**, *19*, 4778.

(86) Wu, H.; Lattuada, M.; Sandkühler, P.; Sefcik, J.; Morbidelli, M. Role of Sedimentation and Buoyancy on the Kinetics of Diffusion-Limited Colloidal Aggregation. *Langmuir* **2003**, *19*, 10710.

(87) Fitch, R. *Polymer Colloids: A comprehensive introduction*; Academic Press: London, 1997.

(88) Goodwin, J.; Ottewill, R.; Pelton, R. Studies on the preparation and characterization of monodisperse polystyrene latices V: The preparation of cationic latices. *Colloid Polym. Sci.* **1979**, *257*, 61.

(89) Lin, M.; Klein, R.; Lindsay, H.; Weitz, D.; Ball, R.; Meakin, P. The Structure of Fractal Colloidal Aggregates of Finite Extend. *J. Colloid Interface Sci.* **1990**, *137*, 263.

(90) Romero-Cano, M.; Martin-Rodriguez, A.; Chauveteau, G.; de las Nieves, F. Colloidal Stabilization of Polystyrene Particles by Adsorption of Nonionic Surfactants I. Adsorption Study. *J. Colloid Interface Sci.* **1998**, *198*, 266.

(91) Sefcik, J.; Verduyn, M.; Storti, G.; Morbidelli, M. Charging and colloidal stability of electrostatically stabilized latex particles. *Prog. Colloid Polym. Sci.* **2004**, *126*, in press.